Palaeogeography, Palaeoclimatology, Palaeoecology 386 (2013) 669–689

Contents lists available at SciVerse ScienceDirect

Palaeogeography, Palaeoclimatology, Palaeoecology

journal homepage: www.elsevier.com/locate/palaeo

Climate change and decadal to centennial-scale periodicities recorded in a late Holocene NE Pacific marine record: Examining the role of solar forcing

J.M. Galloway [a,*], A. Wigston [a], R.T. Patterson [a], G.T. Swindles [b], E. Reinhardt [c], H.M. Roe [d]

[a] Department of Earth Sciences and Ottawa Geoscience Centre, Carleton University, 1125 Colonel By Drive, Ottawa, Ontario K1S 5B6, Canada
[b] School of Geography, University of Leeds, Leeds LS2 9JT, United Kingdom
[c] School of Geography and Earth Sciences, McMaster University, Hamilton, ON L8S 4K1, Canada
[d] School of Geography, Archaeology and Palaeoecology, Queen's University Belfast, Belfast BT7 1NN, United Kingdom

ARTICLE INFO

Article history:
Received 29 November 2012
Received in revised form 21 June 2013
Accepted 22 June 2013
Available online 4 July 2013

Keywords:
Late Holocene
Climate change
Diatoms
Solar forcing
NE Pacific
Wavelet analysis

ABSTRACT

We present a decadal-scale late Holocene climate record based on diatoms, biogenic silica, and grain size from a 12-m sediment core (VEC02A04) obtained from Frederick Sound in the Seymour-Belize Inlet Complex of British Columbia, Canada. Sediments are characterized by graded, massive, and laminated intervals. Laminated intervals are most common between c. 2948–2708 cal. yr BP and c. 1992–1727 cal. yr BP. Increased preservation of laminated sediments and diatom assemblage changes at this time suggest that climate became moderately drier and cooler relative to the preceding and succeeding intervals. Spectral and wavelet analyses are used to test for statistically significant periodicities in time series of proxies of primary production (total diatom abundance, biogenic silica) and hydrology (grain size) preserved in the Frederick Sound record. Periodicities of c. 42–53, 60–70, 82–89, 241–243, and 380 yrs are present. Results are compared to reconstructed sunspot number data of Solanki et al. (2004) using cross wavelet transform to evaluate the role of solar forcing on NE Pacific climate. Significant common power of periodicities between c. 42–60, 70–89, 241–243, and of 380 yrs occur, suggesting that celestial forcing impacted late Holocene climate at Frederick Sound. Replication of the c. 241–243 yr periodicity in sunspot time series is most pronounced between c. 2900 cal. yr BP and c. 2000 cal. yr BP, broadly correlative to the timing of maximum preservation of laminated sedimentary successions and diatom assemblage changes. High solar activity at the Suess/de Vries band may have been manifested as a prolonged westward shift and/or weakening of the Aleutian Low in the mid-late Holocene, which would have diverted fewer North Pacific storms and resulted in the relatively dry conditions reconstructed for the Seymour-Belize Inlet Complex.

1. Introduction

Glacially scoured marine inlets along the coast of British Columbia (BC) provide unique settings for paleoclimate investigations because the presence of terminal glacially deposited sills restricts the movement of dense, oxygen-rich seawater into inner basins (Thomson, 1981). The estuarine-type circulation common in coastal inlets further restricts circulation in inner basins and the resulting persistent dysoxia in stagnant bottom waters creates an ideal environment for the accumulation and preservation of sedimentary sequences and microfossils. Few paleoecological studies have focused on the marine inlets of BC; Saanich and Effingham Inlets on southeastern and southwestern Vancouver Island, respectively, are the only two marine fjords that have been extensively investigated (Fig. 1; Nederbragt and Thurow, 2001; Chang et al., 2003; Dean and Kemp, 2004; Patterson et al., 2004a, 2004b, 2005; Dallimore et al., 2005; Hay et al., 2007; Ivanochko et al., 2008). Additionally, few continuous decadal-scale resolution records of paleoclimate exist for coastal BC (Nederbragt and Thurow, 2001; Pellatt et al., 2001; Ivanochko et al., 2008; Galloway et al., 2010; Babalola et al., 2013). High-resolution marine paleoclimate records can provide insights into both high and low frequency climate oscillations, and thus provide information not available from the relatively short instrumental record or from centennial-scale proxy reconstructions.

Several cyclic phenomena impact the climate of Pacific Canada today, including the El Niño Southern Oscillation (ENSO) and the longer-lived Pacific Decadal Oscillation (PDO) (Minobe, 1997, 1999; Mantua and Hare, 2002). Solar variability also influences the climate of this region by modulating the relative position and intensity of the Aleutian Low pressure system (AL) (Christoforou and Hameed, 1997) and appears to be the pacemaker of ENSO and PDO events (Mann et al., 2005; Shen et al., 2006; Asmerom et al., 2007; Velasco

* Corresponding author at: Geological Survey of Canada, Calgary, 3303-33rd Street N.W., Calgary, AB T2L 2A7, Canada. Tel.: +1 403 292 7187.
E-mail address: Jennifer.Galloway@NRCan.gc.ca (J.M. Galloway).

0031-0182/$ – see front matter.
http://dx.doi.org/10.1016/j.palaeo.2013.06.031

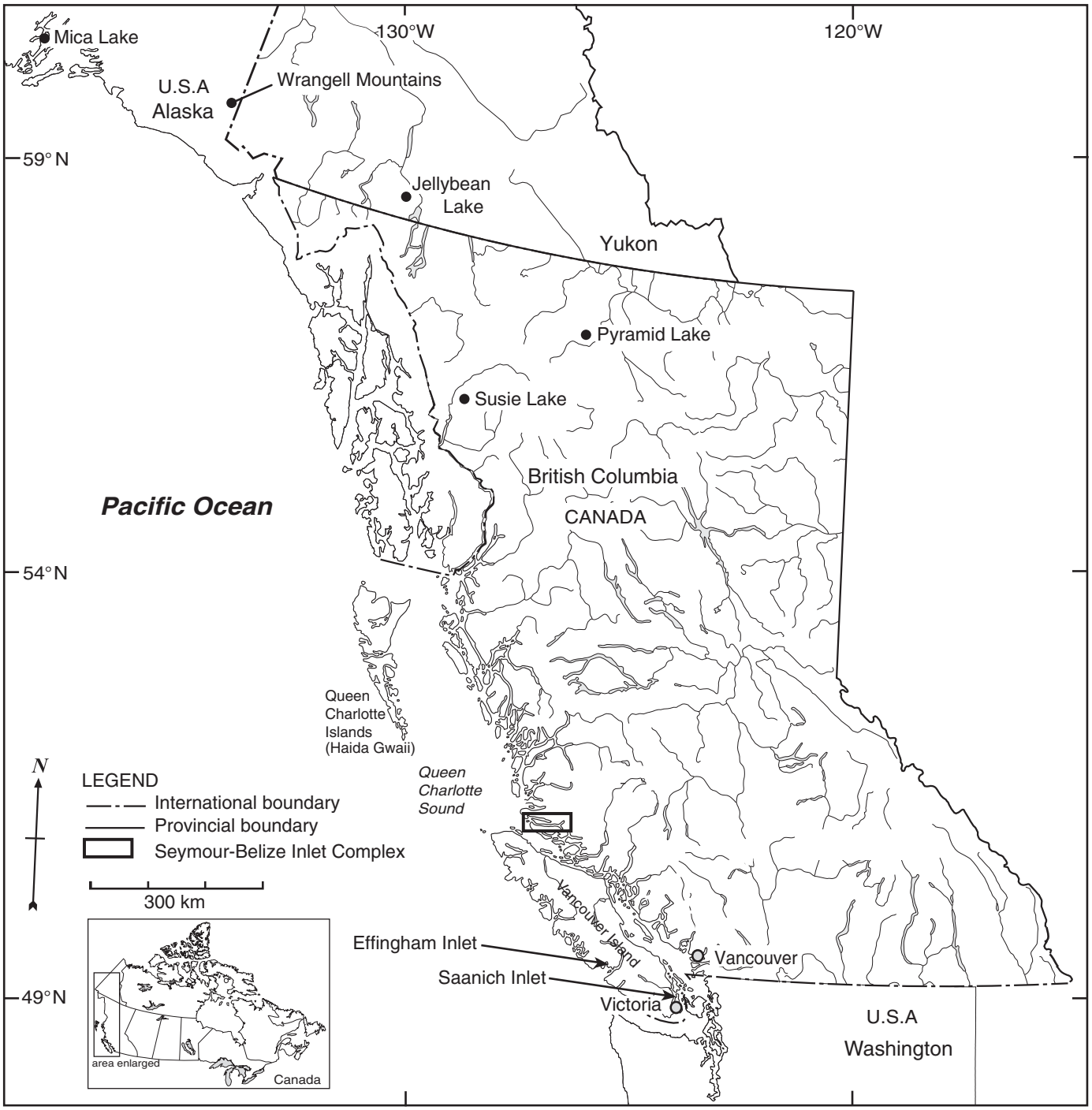

Fig. 1. Map of British Columbia and adjacent areas showing the location of the Seymour-Belize Inlet Complex and study sites mentioned in the text.

and Mendoza, 2008). During the late Holocene, ocean-atmosphere and solar dynamics in the NE Pacific, manifested as changes in the intensity and frequency of oceanic upwelling and winter precipitation in south coastal BC, influenced marine primary production, sedimentation, and fish populations in Effingham and Saanich Inlets (Nederbragt and Thurow, 2001; Dean and Kemp, 2004; Patterson et al., 2004a, 2004b, 2005, 2013; Dallimore et al., 2005; Hay et al., 2003, 2007, 2009; Ivanochko et al., 2008).

The Seymour-Belize Inlet Complex (SBIC) is a network of fjords that penetrate the central mainland coast of BC northward of Effingham and Saanich Inlets (Fig. 2). The SBIC opens to the NE Pacific Ocean via Queen Charlotte Sound and is located adjacent to the oceanic Coastal Transition Domain (Figs. 2, 3; Ware and Thomson, 2000). Because the relative position and strength of the AL have been linked to basin wide ocean circulation patterns, including those associated with the PDO and ENSO (Trenberth and Hurrell, 1994), this near coastal site at the same latitude as the oceanic Coastal Transition Domain is expected to be a sensitive recording area of late Holocene atmospheric dynamics. Further, due also to the unique oceanographic position of the SBIC and because it does not open to the open ocean, the influence of oceanic upwelling is not expected to dominate history of this site, unlike at Effingham and Saanich inlets. Instead, the sedimentary and biological records of the SBIC are expected to represent changes in the watershed.

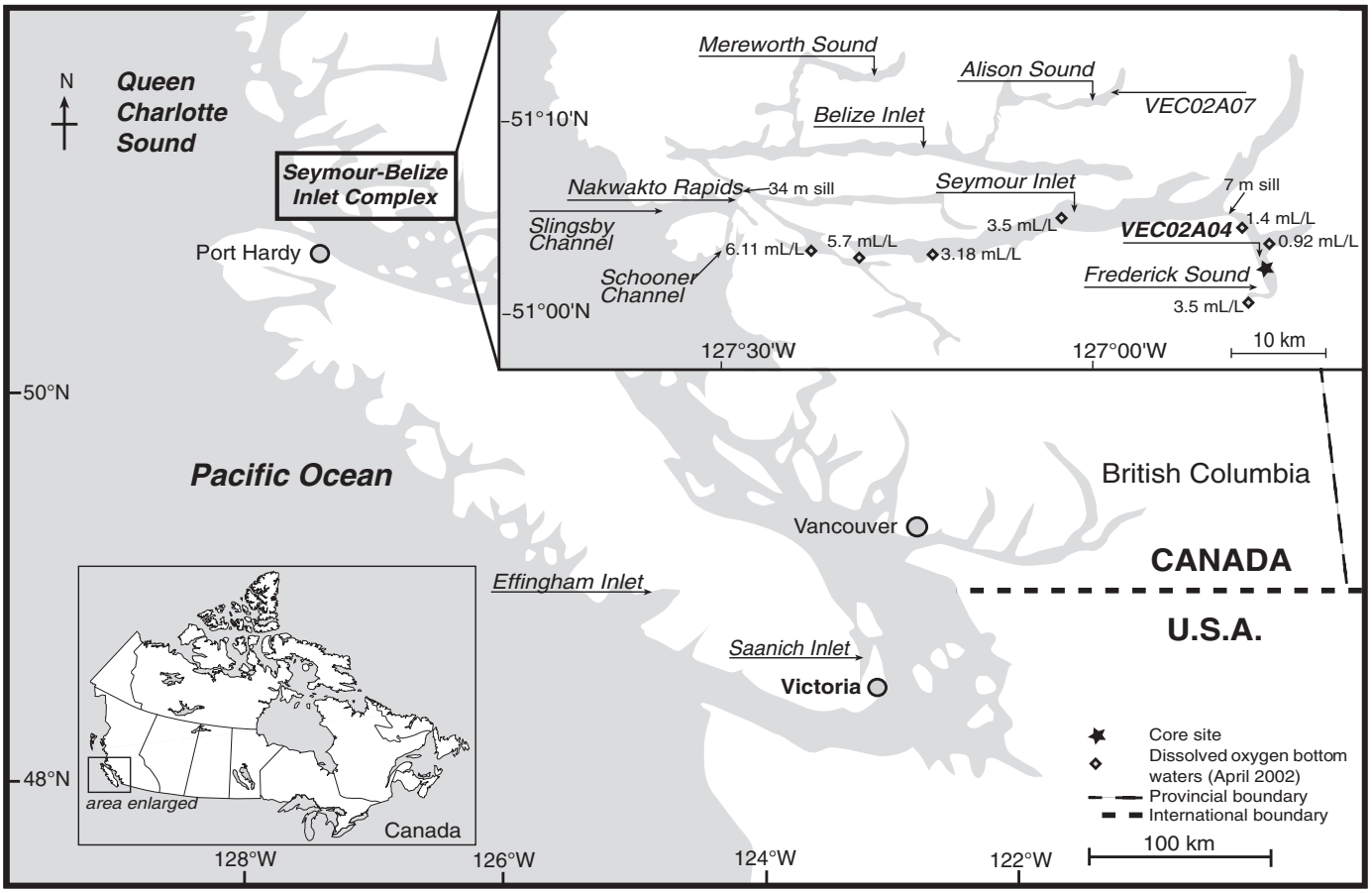

Fig. 2. Map showing the location of the Seymour-Belize Inlet Complex, Frederick Sound, and the core site (VEC02A04). Bottom-water dissolved oxygen measurements also shown. The location of VEC02A07 (Patterson et al., 2007) and FC04 (Vázquez-Riveiros and Patterson, 2009) is shown.

We examine a 12-m long late Holocene-aged sediment core (VEC02A04) from Frederick Sound, a topographically restricted fjord located over 60 km inland from the Pacific Ocean at the SE extent of the SBIC. Foraminifera indicative of oxygenated conditions are absent in this core, confirming that sediments preserved in VEC02A04 were deposited under persistently dysoxic conditions (Babalola, 2009; Babalola et al., 2013). We aim to test the replicability of late Holocene climate documented in sediment records from Saanich Inlet (Dean and Kemp, 2004) and Effingham Inlet (Patterson et al., 2004a, 2004b, 2005; Ivanochko et al., 2008) to evaluate coherence of signals in the distinctive oceanographic and hydrologic setting of the SBIC. We also compare results to climatic periodicities documented from distant sites and to cosmogenic nuclide data (Solanki et al., 2004) to evaluate the influence of allogenic controls on the climate of the Pacific Canada. If periodicities in sediment records from the SBIC are consistent with those documented from other sites in Pacific Canada, distant sites, and proxies of solar activity, it is reasonable to conclude that they were influenced by solar forcing.

2. Regional setting

2.1. Geography

The SBIC forms a 1600 km long network of steep-sided fjords on the central mainland coast of BC between 50°50.2′N and 51°10.6′N, and between 126°30.2′W and 127°40.5′W (Fig. 2). The landscape surrounding the SBIC is rugged and steep, reaching up to 900 m in elevation. Granitic and volcanic rocks of Mesozoic age dominate the bedrock of this region (Meidinger and Pojar, 1991).

2.2. Climate

The climate of the SBIC is cool (mean annual temperature 8.3 °C; range 7.0 °C to 10.1 °C) and wet (mean annual precipitation of 2682 mm; range 1555 mm to 4387 mm; unknown observation period; Green and Klinka, 1994). Seasonal climate and weather systems of the SBIC are largely influenced by the location and intensity of the AL and the North Pacific High pressure system (NPH) that modify the location, timing, and degree of precipitation along the BC coast. The NPH is present year-round and its centre of action is located around 30–40°N latitude off the California coast (Fig. 3). It reaches maximum intensity from June to August when it expands in influence to cover most of the NE Pacific Ocean. From May through September, coastal winds flow in a clockwise direction over the ocean due to the combined effect of a greatly weakened AL and intensified NPH, and are predominantly from the NW. The AL gradually increases in intensity from August to January as its center of action shifts southeastward from the northern Bering Sea to the Gulf of Alaska (Fig. 3). Maximum intensity of the low-pressure cell and its associated counter-clockwise winds occurs in January, when its center of action shifts to over the western Aleutian Islands. After January, intensity of the AL tapers off until July when it is no longer evident in the monthly average surface pressure maps for coastal BC (Thomson, 1981). From late fall (autumn) to early spring when strong cyclonic winds are most prevalent over the NE Pacific ocean, prevailing coastal winds are from the southern quadrant (S, SE, and SW) (Thomson, 1981). The transition to a seasonally strengthened AL and associated southerly winds during fall is accompanied by an increase in the number and intensity of traveling cyclonic disturbances. Storms occur more often and with greater strength in fall and winter than in spring and

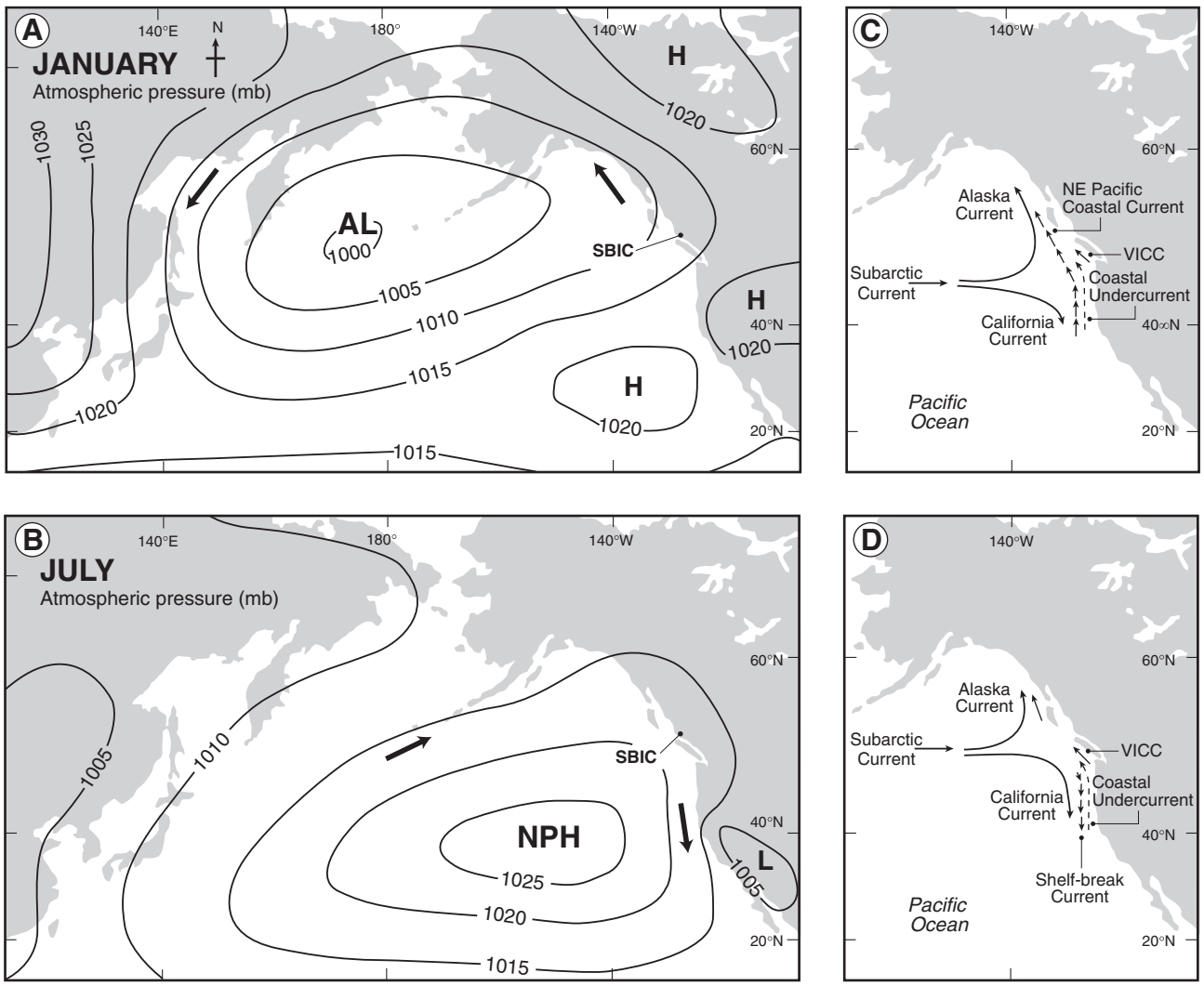

Fig. 3. Maps showing main ocean-atmosphere circulation features for the NE Pacific region in the winter (A,C) and summer (B,D) months. The location of the Seymour-Belize Inlet Complex (SBIC) is shown. Maps after Favorite et al. (1976). In summer, northerly winds associated with the North Pacific High (NPH) generate the southward Shelf-Break Current at surface and consequent offshore Ekman transport induces upwelling. In winter, southerly winds associated with the Aleutian Low (AL) generate a northward drift producing the NE Pacific Coastal Current and consequent onshore Ekman transport that causes an accumulation of low density, less saline water at surface that restricts the upwelling of deep water. The Vancouver Island Coastal Current (VICC) and Coastal Undercurrent are permanent features although they vary in strength seasonally.

summer (Thomson, 1981). The coast of BC thus receives the majority of its precipitation during winter months when a strengthened AL dominates the North Pacific and moisture-bearing storms are advected towards the coast (Miller et al., 1994; Latif and Barnett, 1996).

Regionally modified decadal and centennial-scale cycles that appear to arise from global-scale teleconnections are superimposed on seasonal weather phenomena associated with the AL. One of these longer cycles, the PDO, is a decadal-scale oceanic index of Pacific Ocean sea surface temperatures that oscillates in two general periodicities: one from 15 to 25 yrs and one from 50 to 70 yrs (Minobe, 1997, 1999; Mantua and Hare, 2002). An oxygen isotope record from Jellybean Lake, Yukon Territory (Fig. 1), shows that atmospheric dynamics oscillating on the 50–70 yr cycle have persisted for at least the past c. 200 yrs and lower frequency oscillations of the AL have occurred over at least the last c. 7500 yrs (Anderson et al., 2005). The c. 50 yr cycle is documented in a record of late Holocene marine productivity from Effingham Inlet (Ivanochko et al., 2008). In general, when the AL is on average more eastward and/or intense, westerly winds form a meridional airflow pattern that generates frequent and intense North Pacific storms that are directed to the northern coast of BC and southern Alaska, resulting in relatively warmer and wetter winters in these regions, and leaving the south coast of BC drier than usual. In contrast, a westward positioned and/or weaker AL is associated with a more zonal airflow pattern that does not generate as numerous or intense North Pacific storms. Winters along the northern BC and southern Alaskan coasts are cooler and drier than usual and North Pacific storms that do form tend to be directed to the south coastal BC (Klein, 1949; Leathers et al., 1991; Barron and Anderson, 2011; Hubeny et al., 2011).

2.3. Oceanography

The SBIC extends more than 90 km inland from its mouth at Nakwakto Rapids (Fig. 2). Seaward of Nakwakto Rapids, the SBIC opens to Queen Charlotte Sound and to the NE Pacific Ocean via Slingsby and Schooner Channels (Fig. 2). The SBIC is located adjacent to the oceanic Coastal Transition Domain (Fig. 3). The Subarctic Current and West Wind Drift are large west-to-east surface currents situated at approximately 42°N and 29°N. As they approach North America, the currents bifurcate at the Coastal Upwelling Domain due to divergence in prevailing wind patterns and split into the northern flowing Alaskan Current and the southward flowing California Current (Fig. 3; Ware and McFarlane, 1989). At present,

upwelling conditions prevail in the open water areas outside of the SBIC, but despite strong seaward currents at Nakwakto Rapids, oxygenated waters do not penetrate into the SBIC (Thomson, 1981). At the mouth of the SBIC, at Nakwakto Rapids, there is a sill 300 m wide that extends from the seafloor to 34 m water depth. The bottleneck resulting from this sill makes this the fastest tidal channel in the world (Thomson, 1981) and is such an impediment to water flow into the SBIC that sea level in the inner inlets never equalizes with that of Queen Charlotte Sound during ebb tidal flow (Fisheries and Oceans Canada, 2003). This sill and other similar glacial deposits restrict movement of ocean water into the inner basins of the SBIC, which together with a wedge of low-salinity water caused by riverine input, results in dysoxic bottom water conditions (Thomson, 1981). Consequently, foraminiferal fauna in Alison Sound are presently characterized by low diversities of agglutinated taxa (Vázquez-Riveiros and Patterson, 2009).

2.4. Sea level history

The SBIC has a complex sea-level history due to crustal rebound and migration of a glacioisostatic forebulge (Vázquez-Riveiros et al., 2007; Roe et al., 2013). Following deglaciation of the region, relative sea level (RSL) dropped. A subsequent rise in RSL in the early Holocene did not breach sill elevations of 3.6 m in isolated lake basins in the SBIC. By 2547–2340 cal. yr BP, RSL dropped again and was only 1.49 ± 0.34 m above present mean tide level (Roe et al., 2013). Although the RSL history of the innermost SBIC is likely to have differed from the outer area due to isostatic differences, late Holocene RSL changes in Frederick Sound were probably of similar small magnitude.

2.5. Frederick Sound

Frederick Sound is a 240 m deep inlet restricted from Seymour Inlet of the SBIC by a 7 m sill (Fig. 2). Vertical salinity profiles of Frederick Sound reveal consistent and well-developed stratification (unpublished cruise reports of *CCGS* Vector, 2000, 2002, 2003; Babalola et al., 2013). Oxygen and temperature profiles indicate that Frederick Sound also has a temperature gradient and that bottom waters are persistently dysoxic to anoxic below pressures of 50 to 100 dbars (unpublished cruise reports of *CCGS* Vector, 2000, 2002, 2003).

3. Material and methods

A 12.24-m long piston core (VEC02A04) was retrieved from a depth of 240 m in Frederick Sound in 2004 (Fig. 2). This core was selected for detailed study because 41% of the sediments are laminated. An absence of calcareous foraminifera and membranous remains in VEC02A04 (~5 yr sampling resolution) confirms that the frequency of penetration of dense oxygen-rich waters into Frederick Sound was insufficient to support these microfauna (Babalola, 2009; Vázquez-Riveiros and Patterson, 2009; Babalola et al., 2013). Larger, bioturbating organisms were also likely to have been excluded.

The uppermost 113 cm of sediment from VEC02A04 was lost on recovery. The sediment core was extruded and longitudinally split. Core depth measurements begin at the top of recovered sediments and are not depth-corrected where de-gassing disrupted stratigraphy, for any losses of sediment, or for any graded or massive sedimentary successions. Core slabs were shipped to Carleton University for sub-sampling and cold storage. An archive core is stored at the Pacific Geoscience Centre, Sidney, BC.

3.1. Chronology and age-depth modeling

An age-depth model and total chronological error based on nine AMS radiocarbon dates from terrestrial plant macrofossils were produced using *Bacon* (Fig. 4; Blaauw and Christen, 2011). This age-depth model is based on a piece-wise (5-cm thickness) linear accumulation model where the accumulation rate of sections depends to a degree on that of preceding sections. No corrections were made for different sedimentary facies. To accommodate potential outlying dates, ages were calibrated using a Student's-*t* distribution with default parameters $a = 3$ and $b = 4$ (Christen and Perez, 2009) and the northern hemisphere calibration curve for terrestrial material (Reimer et al., 2009). As prior accumulation rate, we used a gamma distribution with shape 2, a mean accumulation rate of 2.9 yr cm^{-1}, and for memory we used a beta distribution with strength 4 and mean 0.7. A degree of memory is assumed between neighboring depths, with high memory causing near constant accumulation rates and low memory causing more variable rates. Prior information was combined with the radiocarbon dates using thousands of Markov Chain Monte Carlo iterations (Blaauw and Christen, 2011).

3.2. Sedimentary grain size

Two hundred and twenty samples were sub-sampled from VEC02A04 for grain size analysis at 5-cm intervals. Five cubic centimeters of sediment was chemically disaggregated with Calgon solution (1%). Hydrochloric acid and hydrogen peroxide were used to remove carbonates and organic matter. Grain size distribution was measured using a Beckman-Coulter LS 230+ laser particle size analyzer. The Fraunhofer optical model was used (Murray, 2002; van Hengstum et al., 2007). Sedimentary grain size is expected to reflect watershed hydrology that can be related to prevailing climate. Coarser grain sizes are deposited during periods of enhanced terrestrial runoff and fluvial discharge associated with warmer and wetter climates (Campbell, 1998). However, because diatoms and other siliceous organisms were not removed prior to analysis, factors affecting diatom populations could also be represented in the grain size dataset.

3.3. Diatoms and biogenic silica

Sediments were sub-sampled at approximate 10-cm intervals from VEC02A04 for biogenic silica analysis. Biogenic silica was measured at the University of British Columbia following standard procedures (Mortlock and Froelich, 1989). Percent biogenic silica in surface sediments is closely linked to biosiliceous productivity in overlying surface waters (Leinen et al., 1986) and is commonly used as a proxy of primary production (e.g., Ivanochko et al., 2008).

Sediments were sub-sampled at approximate 10-cm intervals from VEC02A04 for diatom analysis. Preparation followed Hay et al. (2003) and Chang (2004). A microsphere solution of known concentration was used to calculate total diatom abundance. Diatoms were identified and enumerated using an Olympus BX-51 stereo light microscope equipped with a differential interference contrast filter. Taxonomic identification and niche categorization (e.g., marine, planktic vs. brackish, benthic) followed Cumming et al. (1995), Campeau et al. (1999), Witkowski et al. (2000), and Pienitz et al. (2003). Between 400 and 500 valves were counted in each sample and the relative abundance (%) and absolute abundance of diatoms (valves gram $sediment^{-1}$) were calculated (Batterbee and Kneen, 2003). Stratigraphically Constrained Incremental Sum of Squares (CONISS) analysis (Grimm, 1987) on square root transformed relative abundance data of all diatoms that occurred ≥1% in one or more sample aided determination of diatom assemblage zones at a sum of squares level of five. The hierarchical nature of cluster analysis requires qualitative decisions concerning criteria for zonation; CONISS provides a quantitative means to assist that characterization (Grimm, 1987). Results were graphed using the computer programs TILIA ver 2.0 and TILIAGraph (Grimm, 1993).

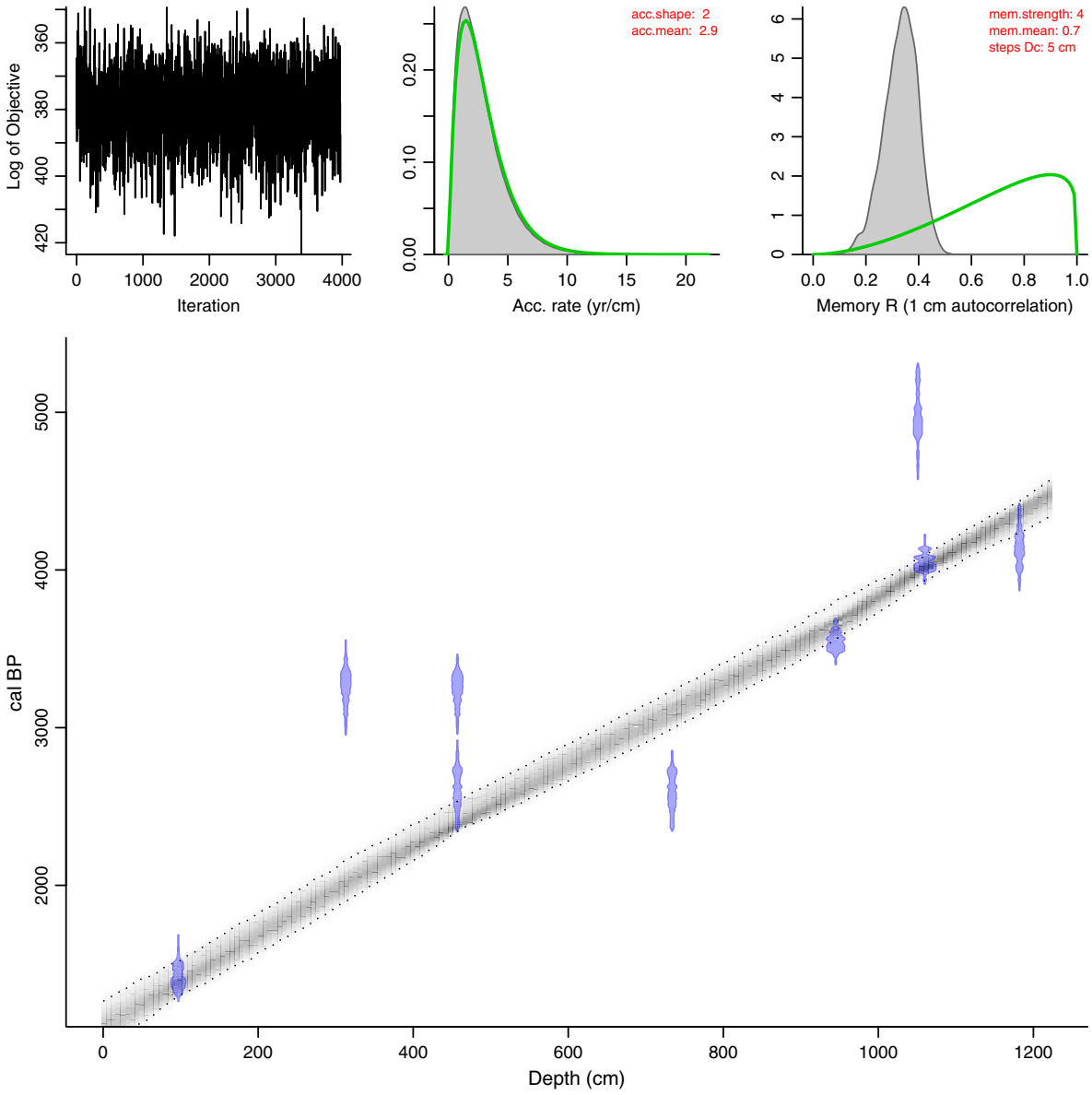

Fig. 4. Bayesian age-depth model developed using *Bacon* for VEC02A04. On the top panel, leftmost plot shows that both MCMC runs were stable (>2000 iterations), middle plot shows the prior (curve) and posterior (filled histogram) distributions for accumulation rate (yr cm^{-1}), and the rightmost plot shows the prior (curve) and posterior (filled histogram) for the dependence of accumulation rate between sections. The large plot shows age distributions of calibrated ^{14}C ages and the age-depth model (grey). Dark grey areas indicate precisely dated sections of the chronology, while lighter grey areas indicate less chronologically secure sections. Bottom graph shows modeled total chronological error range. Chronology is shown in Table 1.

3.4. Wavelet and spectral analyses

Continuous wavelet analysis using a Morlet wavelet was applied to total diatom abundance, biogenic silica, and grain size preserved in VEC02A04 to test time series in the frequency domain (Morlet et al., 1982a, 1982b; Grossman and Morlet, 1984; Torrence and Compo, 1998). Analysis was carried out using PAST software (Hammer et al., 2001). We used spectral analysis (Lomb-Scargle Fourier transform method - REDFIT) to statistically test a null hypothesis of red (autocorrelated) noise in our data (Schulz and Stattegger, 1997; Schulz and Mudelsee, 2002) because red-noise backgrounds pose a particular problem in the analysis of paleoclimate time series (Schwarzacher, 1993). Statistical significance of spectral peaks was tested using a parametric approach (90%, 95%, and 99% false-alarm levels). Time series data were interpolated to an equal interval for wavelet analyses to detect non-stationary periodicities. We applied the same methods to reconstructed sunspot number based on atmospheric radiocarbon ($\Delta^{14}C$, deviation in ‰ from the AD 1950 standard level) derived from decadal samples of absolutely dated tree-ring chronologies (INTCAL98 dataset) (Stuiver and Polach, 1977; Stuiver et al., 1998; Solanki et al., 2004, data available at http://www.ncdc.noaa.gov/paleo/pubs/solanki2004/solanki2004.html) for the period covered by the sediment record preserved in VEC02A04. Fluctuations of ^{14}C on <2000 yr timescales result from variations in ^{14}C production rate in the upper atmosphere of the Earth due to heliomagnetic activity, which modulates cosmic ray flux. Atmospheric ^{14}C may also be affected by changes in the partitioning of carbon between major reservoirs, including the deep ocean, ocean mixed layer, biosphere, and atmosphere. Theoretically, variations in ocean circulation could therefore influence ^{14}C (Broecker, 1994). However, large changes in ocean circulation, such as a slowing down or cessation of thermohaline circulation, need to occur to affect atmospheric ^{14}C due to small

gradients of ^{14}C among reservoirs (Delaygue et al., 2003; Solanki et al., 2004). It is therefore assumed that ^{14}C variations during the late Holocene, when no major oceanic perturbations occurred, can be attributed primarily to solar variability (Solanki et al., 2004). This assumption is supported by the strong similarity of ^{14}C variability to ^{10}Be fluctuations in polar ice cores despite different geochemical behavior and history (Bard et al., 1997; Bond et al., 2001; Solanki et al., 2004).

In climate data, common features in wavelet power of two time series can occur, but at times can be merely a coincidence (Maraun and Kurths, 2004). We use cross wavelet transform of our proxy data and reconstructed sunspot number time series (Solanki et al., 2004) to identify and test the significance of common power using the Cross Wavelet package in Matlab (Hudgins et al., 1993; Torrence and Compo, 1998; Maraun and Kurths, 2004; Grinsted et al., 2004).

4. Results

4.1. Chronology

Total modeled chronological error of VEC02A04 ranges from ±165 to ±315 cal. yr (median ± 240 cal. yr) (Fig. 4). The age of selected horizons in VEC02A04 is estimated from the age-depth model. Based on an average sedimentation rate of 0.39 cm yr^{-1}, the 10-cm sampling interval used for diatoms and biogenic silica is equivalent to c. 26 yrs. The 5-cm sampling resolution used for grain size is equivalent to c. 13 yrs.

Four out of nine radiocarbon ages appear to be outliers (Fig. 4). Dates obtained from two plant macrofossils recovered from a woody layer at 457 cm yield ages that differ by c. 560 cal. yrs. This discrepancy may be due to built-in age effects (McFadgen, 1982;

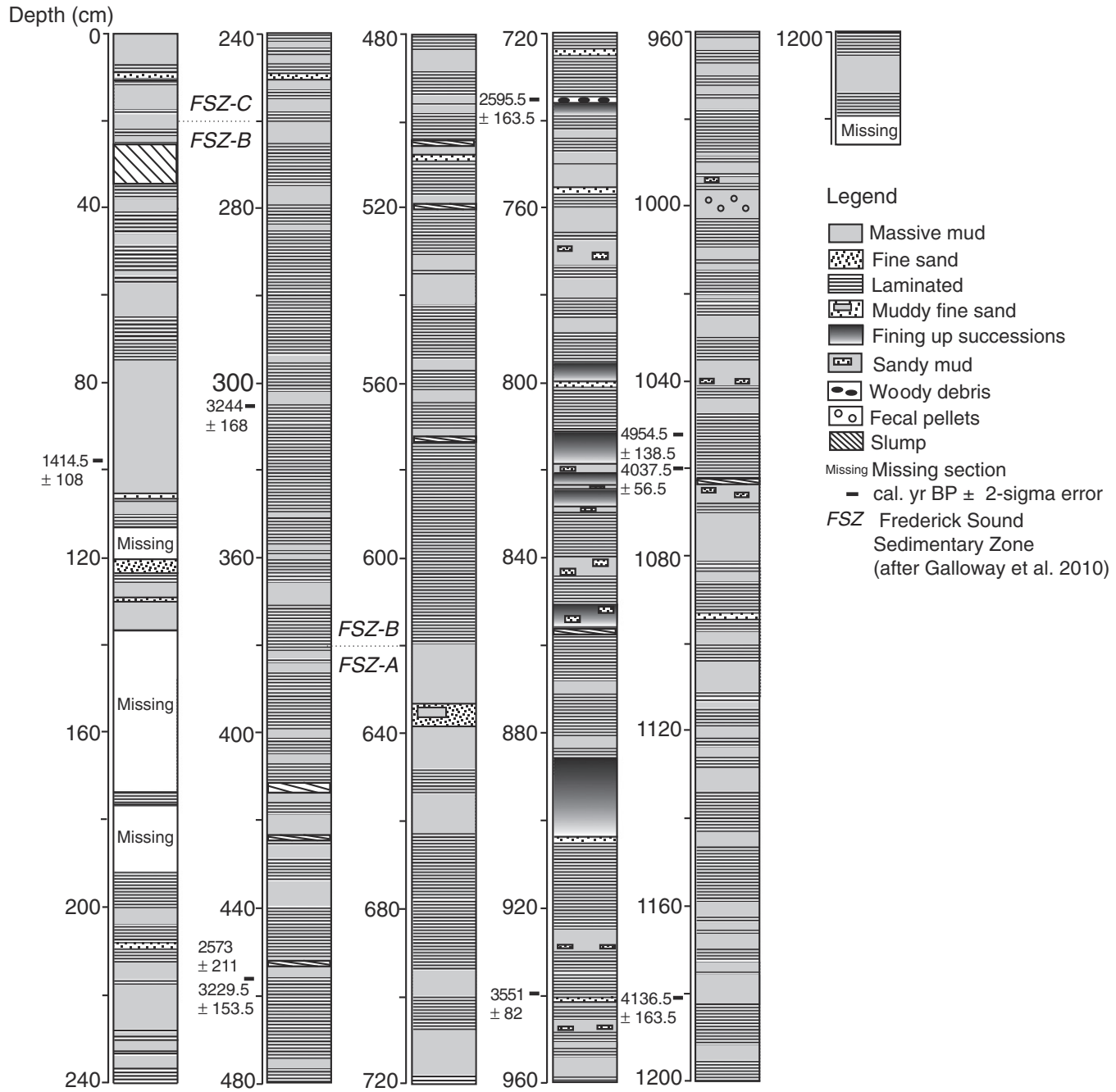

Fig. 5. Sedimentology of the Frederick Sound core (VEC02A04). Sedimentary Zones FSZ-A, FSZ-B, and FSZ-C are shown (Galloway et al., 2010). Chronology is from Table 1.

Oswald et al., 2005) and/or re-deposition of older material. A twig preserved at 1051 cm in VEC02A04 also has an age that appears spuriously old. A twig is unlikely to have built-in age effects because it lacks heartwood and to have originated from reworking of older sediments as it occurs in a laminated interval. Instead, this macrofossil may have survived decomposition for a period of time prior to deposition.

4.2. Sedimentology

Sediments preserved in VEC02A04 are composed of organic-rich dark olive-grey mud and silt with occasional intervals of fine sand. Three sedimentary facies are distributed unevenly in the sediment core: graded sediments (5%); massive sediments (44%); and, laminated sediments (41%) (Fig. 5; Galloway et al., 2010). The remaining 10% of the sediment core is slumped (3%) or missing (7%). Graded intervals are rare, only occur between 905 cm and 740 cm of the core, and show a normally graded succession commencing with sand fining up to mud. Massive sedimentary units range in thickness from a few millimeters to 20 cm, lack internal structure, and are predominantly composed of organic sediments. Massive sediments occasionally contain silt, fine sandy mud, fine sand, fecal pellets, and in one instance, woody debris. Sandy units comprise ~1.2% of the massive sediments and occur as lenses that range in thickness from 1 cm to 5 cm, with the thickest interval occurring between 640 cm and 645 cm of VEC02A04. Continuously laminated successions range in thickness from 1 cm to 45 cm and laminae range in thickness from <0.05 mm to 3 mm. There is no indication of tectonically-derived deposits, such as large slumps (>20 cm), or major disconformities in VEC02A04. Fossil foraminiferal assemblages preserved in VEC02A04 (10-cm sampling resolution) are composed exclusively of species indicative of low oxygen levels [e.g., *Eggerella advena* (Hardwicke), *Spiroplectammina biformis* (Parker and Jones)], indicating that incursions of dense, oxygenated seawater into the inner basin of Frederick Sound were infrequent (Babalola, 2009; Babalola et al., 2013). Persistent low oxygen conditions in fjord bottom waters would have limited bioturbating organisms, and thus, their influence on the sedimentary record.

Stratigraphically constrained cluster analysis of presence or absence data for each sedimentary facies-type aided the identification of three sedimentary zones, FSZ-A, FSZ-B, and FSZ-C (Fig. 5; outlined in Galloway et al., 2010). FSZ-A (c. 4571–4331 cal. yr BP to c. 2958–2708 cal. yr BP) is characterized by numerous massive and graded sediments, FSZ-B (c. 2958–2708 cal. yr BP to c. 1992–1727 cal. yr BP) is characterized by numerous laminated sedimentary successions, and FSZ-C (c. 1992–1727 cal. yr BP to c. 1540–911 cal. yr BP) is comprised of numerous massive sediments (Galloway et al., 2010). Two-way ANOVA and post-hoc analysis (Tukey's HSD test) at the 5% significance level demonstrate that laminated sediments are significantly more common in FSZ-B ($F(2,1147) = 46.7$, $MSE = 10.5$; $M = 0.8 \pm 0.4$ *SD*) than in FSZ-A ($M = 0.5 \pm 0.5$ *SD*) or FSZ-C ($M = 0.5 \pm 0.5$ *SD*).

Grain size declines upcore in VEC02A04. Two-way ANOVA shows that the decline is significant ($F(2,117) = 8.6$, $MSE = 149.6$). Sedimentary grain size is significantly smaller in FSZ-C (Tukey's HSD test, $p < .05$, $M = 62.9$ μm $\pm$ 27.2 *SD*) than in FSZ-B ($M = 79.9$ μm $\pm$ 39.8 *SD*) and FSZ-A ($M = 115.3$ μm $\pm$ 35.4 *SD*).

4.3. Diatoms and biogenic silica

Two hundred diatom species were identified in the 108 samples analyzed, but only 36 had relative abundances ≥1% in at least one sample (Appendix A). Seven of these taxa were assigned an informal species designation; their taxonomy could not be resolved further.

Total diatom abundance ($M = 6.2E+08 \pm 2.4E+08$ *SD* valves gram sediment^{-1}) is similar to diatom concentrations in sediments from other BC inlets (Sancetta, 1989; McQuoid and Hobson, 2001; Chang et al., 2003; Hay et al., 2003; Chang, 2004; Chang and Patterson, 2005; Hay et al., 2007). Dominant diatom species (≥5% abundance in at least two samples) are represented, in descending order, by:

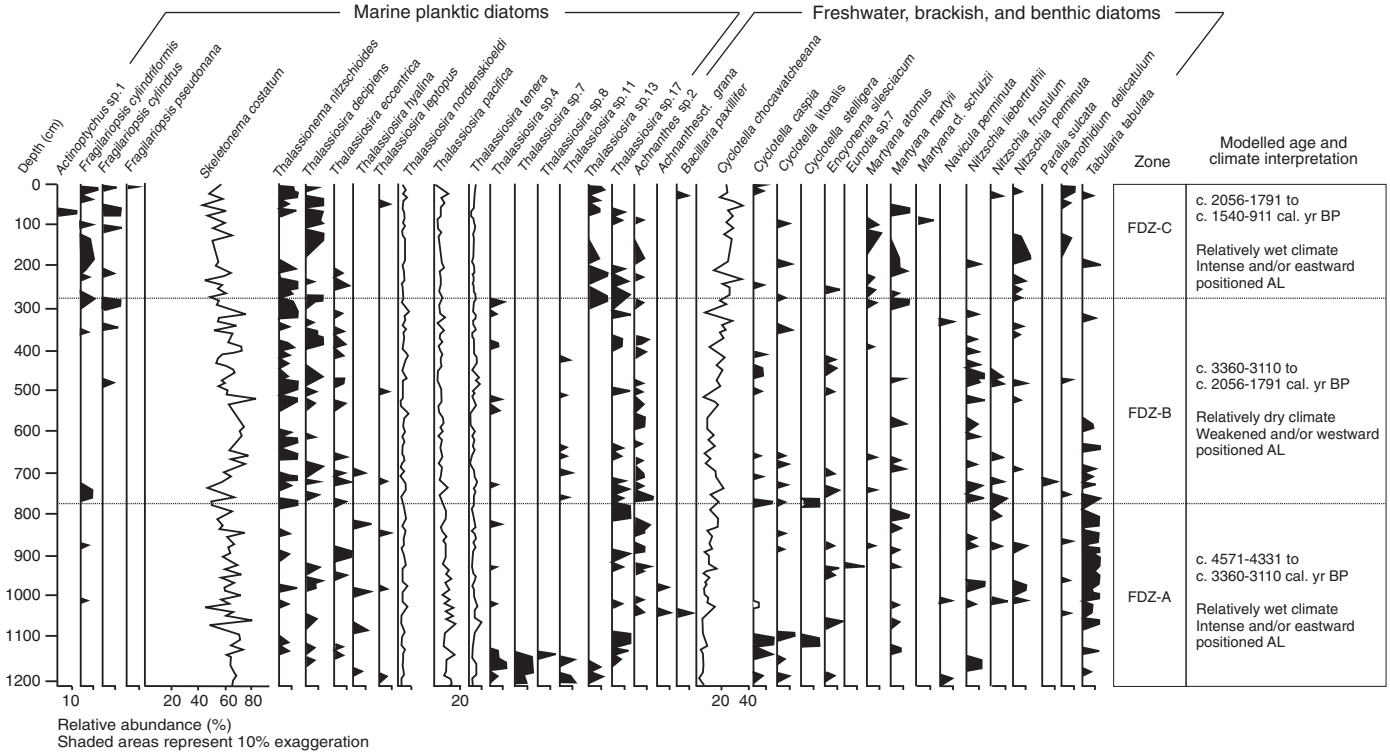

Fig. 6. Relative abundances of diatom taxa occurring ≥1% in one or more sample. Zonation is based on stratigraphically constrained cluster analysis (CONISS) of diatom taxa shown (Grimm, 1987). AL — Aleutian Low pressure system. Chronology is from Table 1 and Fig. 3.

Skeletonema costatum, *Cyclotella choctawatcheeana*, *Thalassiosira pacifica*, *Thalassiosira nordenskioeldii*, and *Thalassiosira tenera*. These five taxa comprise ~90% of the total diatom abundance.

Relative abundances of dominant and minor taxa are shown in Fig. 6 and a five-sample moving average is used to visualize trends in the absolute abundance of the dominant taxa (Fig. 7). *Skeletonema costatum*, *Thalassiosira nordenskioeldii*, *Thalassiosira pacifica*, and *Thalassiosira tenera* display an overall up-core decrease in relative and absolute abundance, while the abundance of *Cyclotella choctawatcheeana* increases up-core (Figs. 6, 7). Overprinted on these trends are higher frequency variations in diatom abundances. We used stratigraphically constrained cluster analysis of the relative abundance of diatom taxa occurring ≥1% in at least one sample to aid the delineation of diatom assemblage zones to better understand these changes. Three diatom assemblage zones were identified: FDZ-A through FDZ-C (Fig. 5). FDZ-A (1219 cm–780 cm; c. 4571–4331 cal. yr BP to c. 3360–3110 cal. yr BP) is characterized by *S. costatum* abundances near 65% and 4.5E+08 valves gram sediment^{-1}. This taxon declines at the end of this zone to ~50% and ~3.5E+08 valves gram sediment^{-1}. *Cyclotella chocawatcheeana* increases in FDZ-A from ~10% to ~20% and ~4.0E+07 to 1.7E+08 valves gram sediment^{-1}. Relative and absolute abundances of *T. pacifica* (~10–15%, ~6.0E+07 valves gram sediment^{-1}) and *T. tenera* (~5%, ~2.5E+07 valves gram sediment^{-1}) are high compared to those in overlying sediments. *Tabularia tabulata* is frequently present in this zone. FDZ-B (780 cm–280 cm; c. 3360–3110 cal. yr BP to c. 2056–1791 cal. yr BP) is characterized by an initial decline in *C. chocawatcheeana* to ~10% and ~3.0E+07 valves gram sediment^{-1} following its peak near the end of FDZ-A. The abundance of *C. chocawatcheeana* then exhibits a gradual increase to ~30% or ~1.7E+08 valves gram sediment^{-1} near the end of FDZ-B. *Thalassiosira pacifica* declines in this zone to less than 10% and 3.0E+07 valves gram sediment^{-1}. The abundance of *S. costatum* occurs near ~70% between 700 and 500 cm in FDZ-B and reaches a core maximum of ~85% and ~1.3E+09 valves gram sediment^{-1} mid-zone, although its mean relative and absolute abundances remain similar to Zone FDZ-A (Figs. 6, 7). FDZ-C (280 cm–0 cm; c. 2056–1791 cal. yr BP to c. 1540–911 cal. yr BP) is characterized by an increase in the relative and absolute abundance of *C. chocawatcheeana* to between 20 and 40%

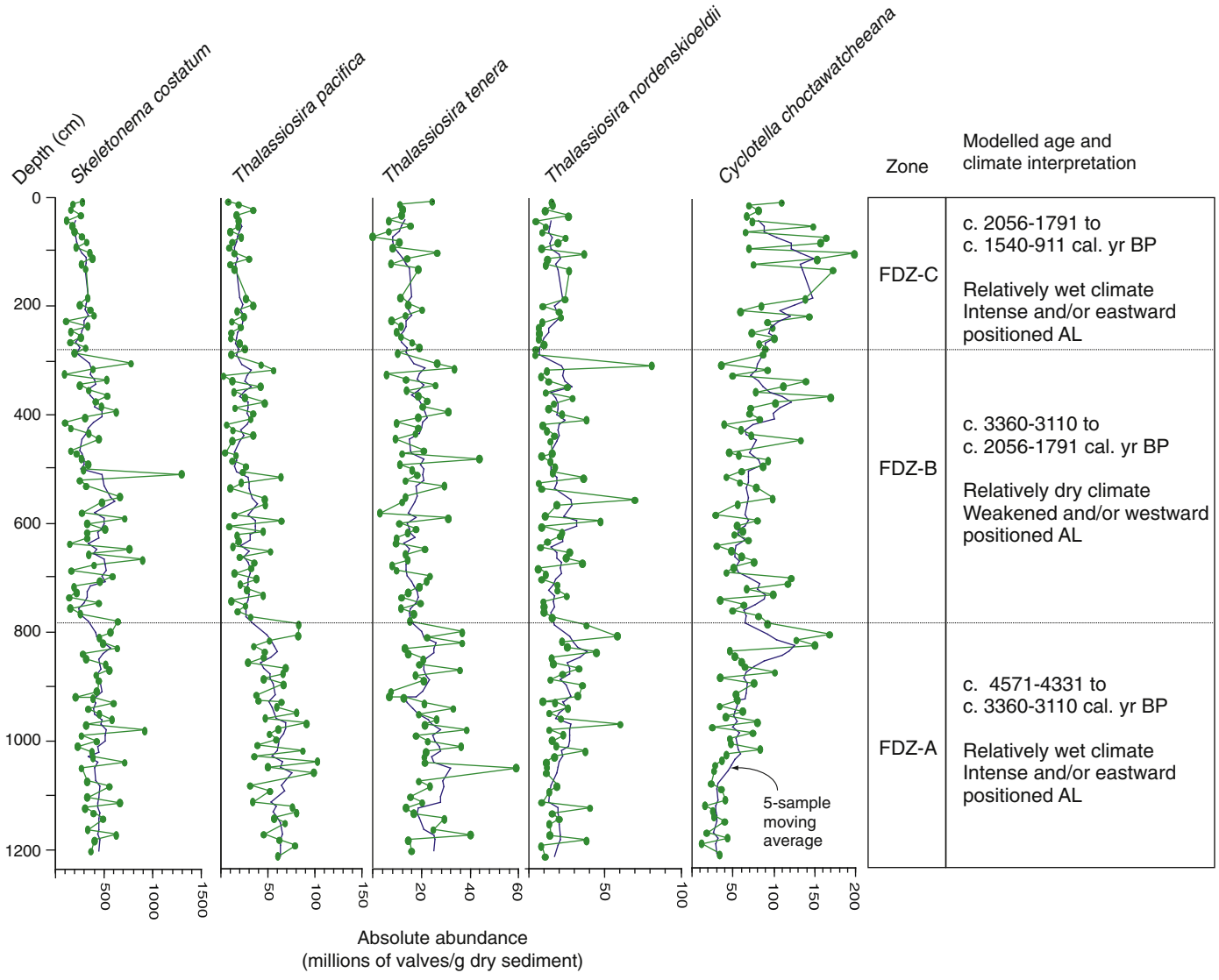

Fig. 7. Absolute abundance of major diatom taxa occurring ≥5% in one or more sample. Zonation is based on stratigraphically constrained cluster analysis (CONISS) of the relative abundance of diatom taxa occurring ≥1% in one or more sample (Grimm, 1987). AL — Aleutian Low pressure system. Chronology is from Table 1 and Fig. 3.

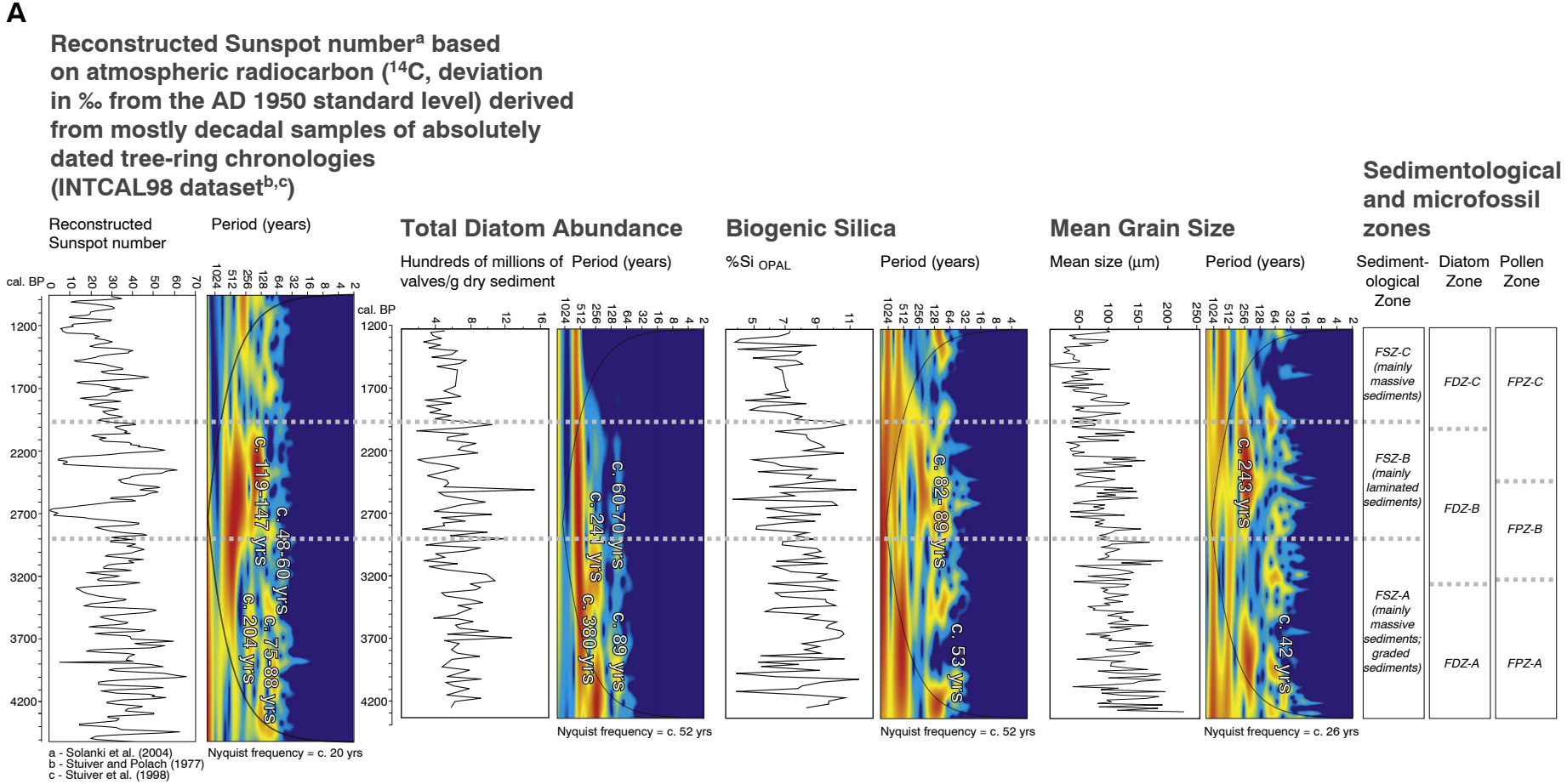

Fig. 8. A — Wavelet analysis total diatom abundance (hundreds of millions of valves gram sediment^{-1}), biogenic silica (%Si_{OPAL}), and mean grain size (µm) preserved in the Frederick Sound sediment core VEC02A04. Dashed line shows cone of influence (Torrence and Compo, 1998) of edge effects. Wavelet analysis of reconstructed sunspot number based on atmospheric radiocarbon (Δ^{14}C, deviation in ‰ from the AD 1950 standard level) derived from mainly decadal samples of absolutely dated tree-ring chronologies (INTCAL98 dataset) (Stuiver and Polach, 1977; Stuiver et al., 1998; Solanki et al., 2004, data available at http://www.ncdc.noaa.gov/paleo/pubs/solanki2004/solanki2004.html). Numbers in scalogram indicate wavelengths exceeding confidence limits for red noise, determined using REDFIT analysis and labeled (in cal. yrs). Sedimentary Zones FSZ-A, FSZ-B, and FSZ-C are delineated by grey dashed lines. The Nyquist frequency, the maximum input frequency that can be resolved in a time series (Davis, 1986), is c. 52 yrs for total diatom abundance and biogenic silica data. For grain size data the Nyquist frequency is c. 26 yrs. Chronology is from Table 1 and Fig. 3. B — Spectral analysis of proxies analyzed in VEC02A04: total diatom abundance (hundreds of million of valves gram sediment^{-1}), biogenic silica (%Si_{OPAL}), and mean grain size (µm) and reconstructed sunspot number based on atmospheric radiocarbon (Δ^{14}C, deviation in ‰ from the AD 1950 standard level) derived from mainly decadal samples of absolutely dated tree-ring chronologies (INTCAL98 dataset) (Stuiver and Polach, 1977; Stuiver et al., 1998; Solanki et al., 2004, data available at http://www.ncdc.noaa.gov/paleo/pubs/solanki2004/solanki2004.html). Peaks exceeding confidence limits for red noise, determined using REDFIT analysis, are labeled (in cal. yrs). Chronology is from Table 1 and Fig. 3.

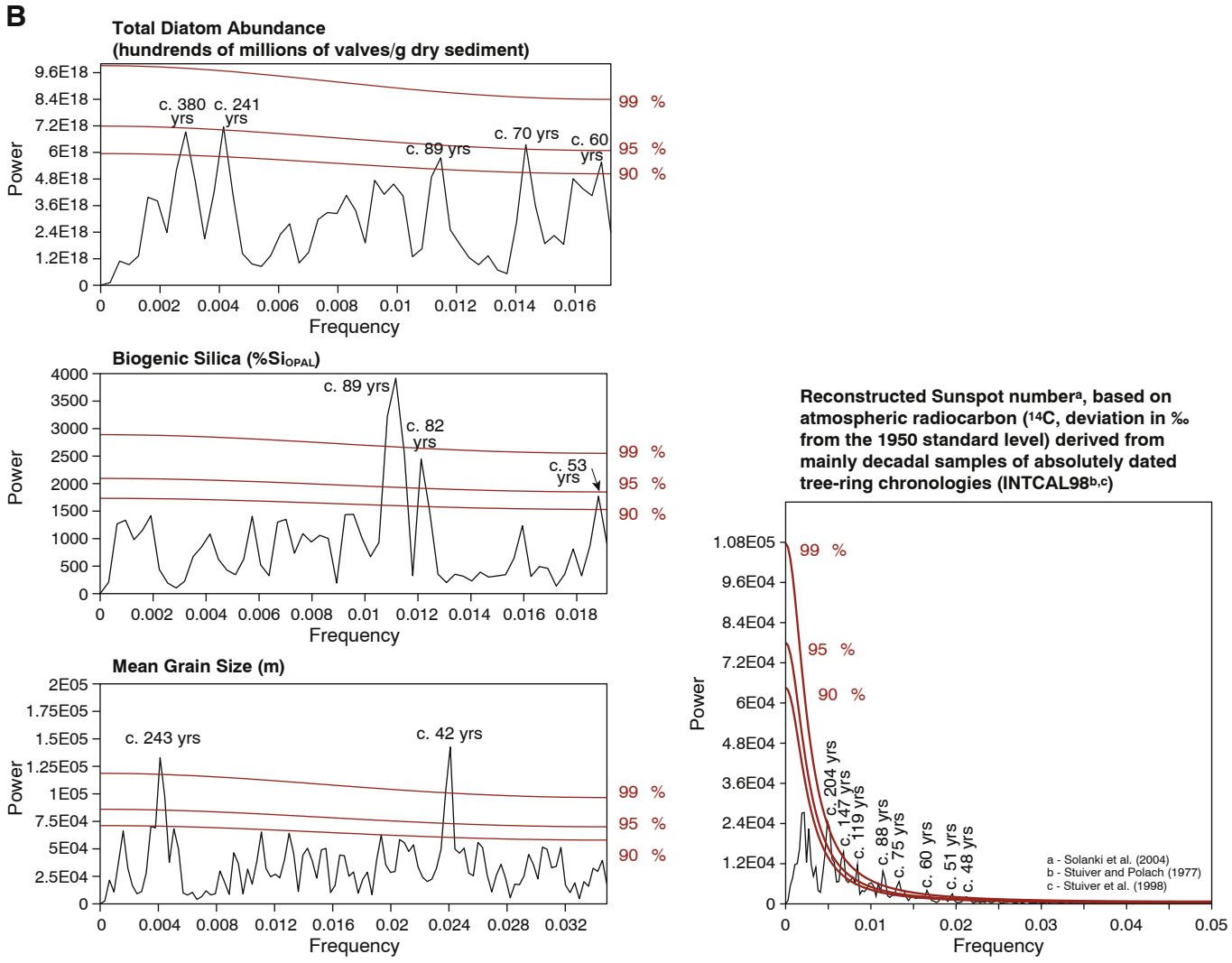

Fig. 8 (*continued*).

and 6.0E+07 and 2.0E+08 valves gram sediment^{-1}. *Skeletonema costatum* declines to ~55% and ~2.6E+08 valves gram sediment^{-1}. The benthic diatoms *Martyana* spp., *Fragilariopsis cylindriformis*, *Fragilariopsis cylindrus*, and *Planothidium delicatulum* are commonly present in this zone.

Total diatom abundance and biogenic silica decline in the uppermost portion of VEC02A04. One way ANOVA and post-hoc analysis (Tukey's HSD test, $p < .05$) show that total diatom abundance ($F(2,213) = 10.3$, $MSE = 5.4E+17$) and biogenic silica ($F(2,117) = 8.6$, $MSE = 149.6$) are significantly lower in FSZ-C ($M = 4.9E+08$ valves gram sediment^{-1} ± 1.4E+08 *SD*, $M = 15.3$ %Si$_{OPAL}$ ± 3.6 *SD*) than in FSZ-A ($M = 6.7E+08$ valves gram sediment^{-1} ± 2.3E+08 *SD*, $M = 19.5$ %Si$_{OPAL}$ ± 4.3 *SD*) and FSZ-B ($M = 6.1E+08$ valves gram sediment^{-1} ± 2.8E+08 *SD*, $M = 19.1$ %Si$_{OPAL}$ ± 4.3 *SD*).

4.4. Time series analyses

Spectral analysis demonstrates that total diatom abundance, biogenic silica, and grain size time series have significant variability on decadal to centennial times scales that cannot be explained by first-order autoregressive processes (Figs. 8A, B). Significant signals of c. 60, 70, 89, 241, and 380 yrs occur in total diatom abundance time series (Fig. 8B). Wavelet analysis shows that these signals are most pronounced in FSZ-A and the beginning of FSZ-B before becoming nonexistent or weak in FSZ-C (Fig. 8A). Periodicities of c. 53, 82, and 89 yrs are significant in biogenic silica time series (Fig. 8B). The c. 42 yr cycle is most pronounced in FSZ-A and FSZ-B and the c. 82–89 yr cycle persists into FSZ-C (Fig. 8A). Significant periodicities of c. 42 and 243 yrs occur in grain size data (Fig. 8B). The c. 42 yr cycle is most pronounced in FSZ-A and FSZ-B while the c. 243 yr cycle is most pronounced in FSZ-B (Fig. 8A). Periodicities of c. 48, 51, 60, 75, 88, 119, 147, and 204 yrs are significant in reconstructed sunspot number time series (Fig. 8B). We emphasize the lower frequency signals detected in total diatom abundance, biogenic silica, and grain size time series because Nyquist frequencies of c. 26 to 52 yrs approach the highest frequencies signals of c. 42–60 yrs.

Cross wavelet transform of total diatom abundance, biogenic silica, and grain size with reconstructed sunspot number time series (Solanki et al., 2004) demonstrates significant common power within c. 42–60, 70–89, and 204–243 yr bands (Fig. 9). The c. 380 yr cycle present in total diatom abundance time series is also significant at the 5% level even though this wavelength does not peak above the 90% C.I. in reconstructed sunspot number time series (Fig. 8B). Common power at the c. 42–60 and 70–89 yr bands is intermittent throughout the VEC02A04 sediment record while the c. 204–243 yr band is significant between c. 2900 cal. yr BP and c. 2000 cal. yr BP (Fig. 9).

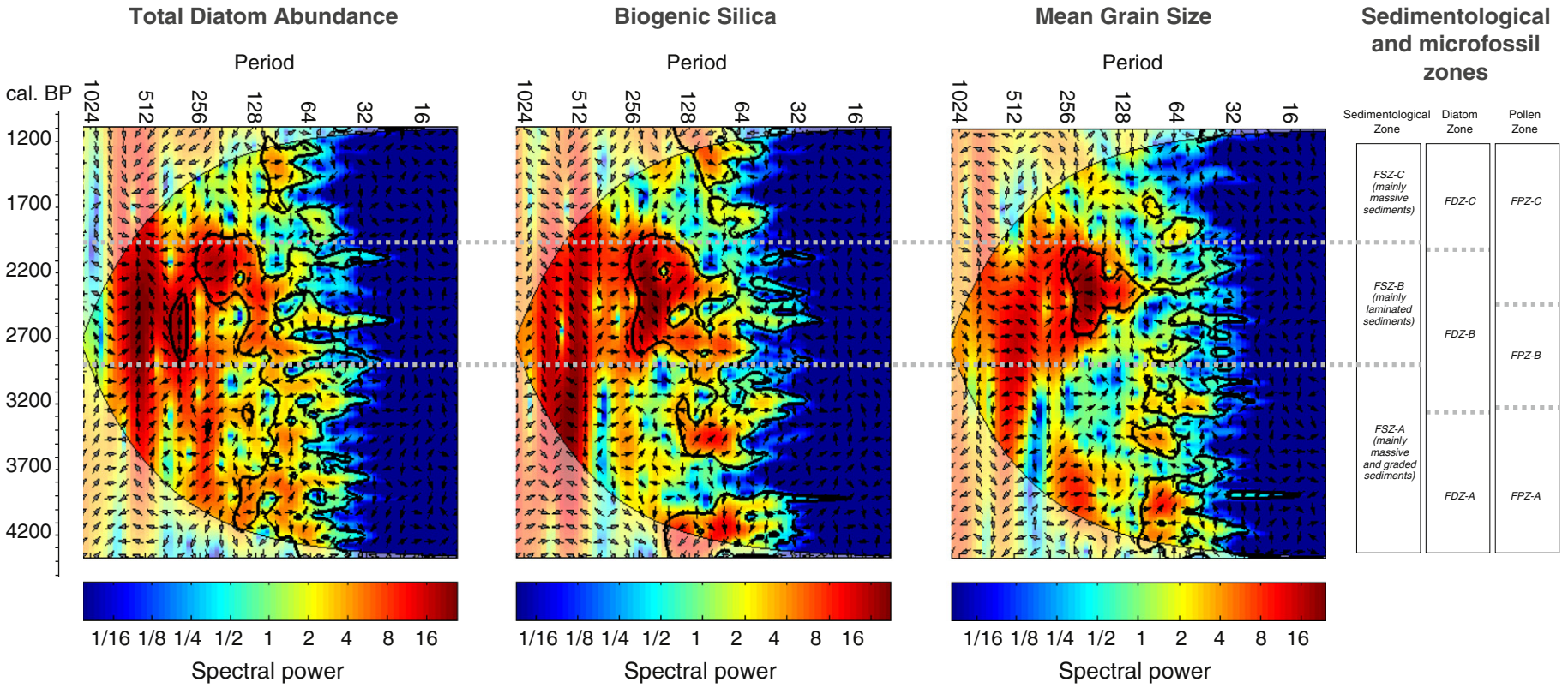

Fig. 9. Cross wavelet transform of total diatom abundance, biogenic silica, and grain size time series and reconstructed sunspot number (Solanki et al., 2004). The 5% significance level against red noise is shown by the black contour. Relative phase relationships are shown as arrows with in-phase pointing right, anti-phase pointing left, and proxy data leading reconstructed sunspot number by 90° pointing straight down. Chronology is from Table 1 and Fig. 3. Sedimentological (FSZ), diatom (FDZ), and pollen zones (FPZ, from Galloway et al., 2010) shown at right.

5. Discussion

5.1. Sedimentology

5.1.1. Non-laminated sedimentary successions

Following the model outlined in Patterson et al. (2007) and discussed in Galloway et al. (2010), we interpret non-laminated sediments, most common in FSZ-A and FSZ-C, to have been deposited by transfer of sediments from fjord sides and/or by re-suspension of basin sediments initiated by localized failure of sediments on the walls of the fjord. Sedimentary deposits formed in this way are expected to occur most frequently during periods of high sedimentation associated with enhanced runoff, fluvial discharge, and freshet and/or incursions of waters into the inner basin of the fjord that affect the stability and consolidation of sediments on steep-sided fjord walls. In general, warm and wet climates result in higher clastic input into marine basins by increasing the weathering rate of catchment soils and rocks, terrestrial erosion rates, and sediment delivery during periods of enhanced freshet, surface runoff, and fluvial input, than during dry climates. Incursions of seawater into the inner basin of Frederick Sound, though rare, may have occurred during wet climate regimes when brackish surface water conditions enhanced stratification in the water column and increased two-layer estuarine circulation. Seawater incursions can create currents and infrequently carry sediment loads that affect the stability of sediments on fjord walls. Massive sedimentary successions are most common in FSZ-A and FSZ-C, and graded sedimentary successions occur only in FSZ-A (Fig. 5), suggesting that a relatively high-energy regime prevailed during deposition of these units between c. 4571–4331 cal. yr BP and c. 2958–2708 cal. yr BP (FSZ-A) and between c. 1992–1727 cal. yr BP and c. 1540–911 cal. yr BP (FSZ-C).

5.1.2. Laminated sedimentary successions

Laminated sediments are most common in FSZ-B (c. 2948–2708 cal. yr BP to c. 1992–1727 cal. yr BP; Fig. 5). We assume that the bulk composition of the laminae and pattern of deposition are the same as have been observed at similar fjords along the BC coast where laminae are composed of alternating light-colored diatom-rich layers and dark-colored terrigenous mineral material (Sancetta and Calvert, 1988; Sancetta, 1989; McQuoid and Hobson, 2001; Chang et al., 2003; Dean and Kemp, 2004). The terrigenous component of an annual laminated couplet is deposited during autumn to spring when a seasonal increase in precipitation results in enhanced terrestrial runoff, fluvial discharge, and freshet, and diatom production is reduced in response to decreased light incidence and cold water temperatures (Sancetta, 1989; Chang et al., 2003). The diatomaceous component of an annual couplet is deposited during the late spring and summer when greater light intensity and relatively warm and dry conditions that promote productivity prevail (Chang et al., 2003; Sancetta, 1989). A decrease in terrigenous sediment supply as a result of a reduction in riverine input, freshet volume, terrestrial runoff, and coastal erosion during relatively dry climates is expected to increase the preservation potential of laminae by reducing the frequency of slope sediment disruption (Patterson et al., 2007). Preservation of laminated sedimentary intervals is also influenced by slope gradient that is, in turn, dependent on sediment particle size, geometry, density, and water content (Patterson et al., 2007). Changes in sea level also affect slope gradient and the probability of laminae being preserved (Patterson et al., 2007). A reduction of relative sea level to 1.49 ±0.34 m above present mean tide level occurred at c. 2547–2340 cal. yr BP (Roe et al., 2013). A relative sea level fall of even this small magnitude, may have further limited the frequency of incursions of sediment-bearing waters across the shallow sill at the mouth of Frederick Sound, resulting in a reduction of this mode of slope disturbance during deposition of FSZ-B and FSZ-A.

5.2. Diatoms and climate change in the NE Pacific

5.2.1. The early-late Holocene (FDZ-A; c. 4571–4331 cal. yr BP to c. 3360–3110 cal. yr BP)

The marine planktic diatoms *Thalassiosira pacifica* and *Thalassiosira tenera* are relatively abundant in VEC02A04 during the early-late Holocene (FDZ-A, c. 4571–4331 cal. yr BP to c. 3360–3110 cal. yr BP). *Thalassiosira* spp. are adapted to low light conditions and cool surface waters and are a typical spring bloom taxon in coastal BC (Waite et al., 1992; Chang, 2004). High relative abundances of these taxa therefore suggest that cool conditions persisted into the late spring and early summer at Frederick Sound in the early-late Holocene. The brackish diatom *Cyclotella choctawatcheeana* begins to increase in the early-late Holocene. This taxon can be used as an indicator of precipitation and runoff in coastal BC fjords because its distribution is limited by high salinities (>20‰; Häkansson et al., 1993; Ryves et al., 2004). The occurrence of *C. choctawatcheeana* in BC fjords has a strong seasonal restriction: Sancetta (1989) observed this taxon to account for up to 20% of all diatoms present during July and August, when surface waters are warm (between 17 °C and 21 °C), surface salinities are low (between 11.5‰ and 13.6‰), and waters are strongly stratified due to enhanced freshwater input via snow-melt and runoff. The relative abundance of *C. choctawatcheeana* in VEC02A04 reaches ~20% by c. 3360–3110 cal. yr BP, likely in response to progressively increasing precipitation, riverine input, and/or enhanced spring freshet during the early-late Holocene at Frederick Sound that reduced surface water salinity. Numerous massive and graded sedimentary successions in FSZ-A indicate that clastic sediment supply was relatively high and frequently resulted in slope failure in Frederick Sound. Relatively frequent slope failure events would have increased turbidity in the water column, resulting in lower light conditions that would have promoted *C. choctawatcheeana* and disrupted production of marine planktic bloom species such as *Skeletonema costatum*, which declines in the VEC02A04 sediment record near c. 3360–3110 cal. yr BP (Smayda, 1973; Hitchcock and Smayda, 1977; Sancetta, 1989; Hay et al., 2003, 2007, 2009). The brackish, benthic diatom *Tabularia tabulata* is frequently present in FDZ-A. This benthic diatom would have been deposited in the basin centre by movement from shallow water environments on the sides of the basin, where it lived, by slope failure events or runoff (Patterson et al., 2013).

Cool and wet climatic conditions in the SBIC may have been influenced by the development of a relatively intense and/or eastward positioned AL in the early-late Holocene. The associated meridional airflow pattern would have diverted North Pacific storms northward to the central and northern coasts of BC, resulting in wet, cloudy, and cool conditions in these regions and leaving the southern coast of BC drier than usual (Barron and Anderson, 2011). The oxygen isotope record from Jellybean Lake, Yukon Territory, documents a predominantly eastward and/or intense AL between c. 4500 cal. yr BP and c. 3000 cal. yr BP (Anderson et al., 2005; Fig. 10).

5.2.2. The mid-late Holocene (FDZ-B; c. 3360–3110 cal. yr BP to c. 2056–1791 cal. yr BP)

A disruption of the increasing trend of *C. choctawatcheeana* and increased preservation of laminated sedimentary successions suggest that freshwater input from direct precipitation, riverine input, freshet, and terrestrial runoff into Frederick Sound was reduced at c. 3360–3110 cal. yr BP. *Skeletonema costatum* reaches peak abundance in VEC02A04 in FDZ-B. *Skeletonema costatum* requires relatively warm, saline waters (Smayda, 1973) and high light incidence (Hitchcock and Smayda, 1977) for maximum production. These diatom and sedimentary changes suggest that a period of relatively warm and dry late spring/early summer climatic conditions occurred during the mid-late Holocene at Frederick Sound. A decline in the abundance of Cupressaceae pollen in VEC02A04 between c. 3269–

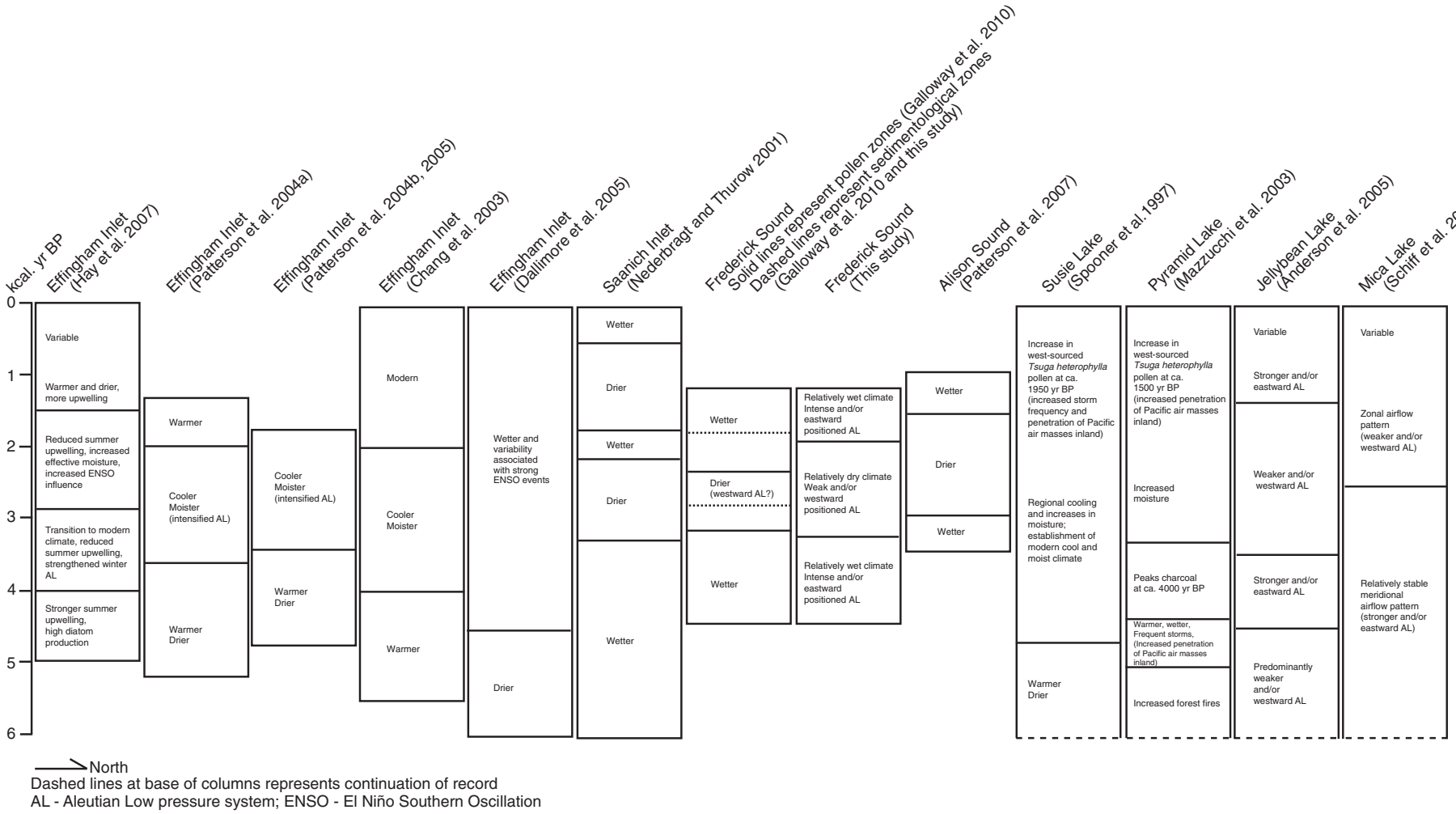

Fig. 10. Summary diagram showing late Holocene climate histories interpreted from this study and selected sites in northwestern North America. Changes in late Holocene atmospheric circulation interpreted from $\delta^{18}O$ values of lacustrine carbonates from Jellybean Lake (Anderson et al., 2005) and of diatom valves from Mica Lake (Schiff et al., 2009) are also shown.

3019 cal. yr BP and c. 2413–2183 cal. yr BP also provides evidence that the climate of Frederick Sound became drier in the mid-late Holocene (Fig. 10; Galloway et al., 2010). A moderate increase in the abundance of thecamoebians, freshwater protists that inhabit salt marshes adjoining the SBIC (Vázquez-Riveiros et al., 2007), in VEC02A04 between 3371–3121 cal. yr BP and 2192–1922 cal. yr BP may also indicate the development of drier climatic conditions in the SBIC (Babalola et al., 2013). Subaerial exposure of marsh substrate may have occurred during drier climatic conditions, resulting in increased erosion of sediment from these environments into Frederick Sound (Babalola et al., 2013). Changes in foraminifera assemblages in VEC02A04 at c. 3199–2954 cal. yr BP suggest that bottom waters in Frederick Sound became cooler in the mid-late Holocene than during the preceding interval.

A broadly synchronous dry mid-late Holocene climate interval is inferred from a reduction in grain size, marine productivity, and changes in other sedimentary features in a sediment record (VEC02A07) from Alison Sound between c. 3100 cal. yr BP and c. 1650 cal. yr BP (Fig. 10; Patterson et al., 2007).

High-resolution marine sedimentary records from south coastal BC suggest that the mid-late Holocene was a period of climate reorganization as well (Fig. 10). At Saanich Inlet, sheltered from west-sourced precipitation by the rainshadow effect of mountains on southern Vancouver Island, thinner varves accumulated between c. 3250 cal. yr BP and c. 2100 cal. yr BP when drier climate conditions reduced terrigenous sedimentary input and sediment accumulation rates (Nederbragt and Thurow, 2001). On the western side of Vancouver Island, reduced *S. costatum* and *Thalassiosira* spp. production characterize sediments of Effingham Inlet deposited between c. 4000 cal. yr BP and c. 2800 cal. yr BP when diminished summer upwelling, more frequent freshwater input, and cloudier conditions promoted brackish, freshwater, and benthic diatom taxa and limited production of typical spring bloom diatoms (Hay et al., 2007). In another study from Effingham Inlet, Chang et al. (2003) identified an increase in non-laminated intervals between c. 4000 cal. yr BP and c. 2200 cal. yr BP, interpreted to indicate that precipitation was likely to have been higher during this interval.

The Jellybean Lake oxygen isotope record documents a steady westward shift and/or weakening of the AL that began at c. 3500 cal. yr BP (Anderson et al., 2005). Schiff et al. (2009) document excursions to lower $\delta^{18}O$ in diatom valves from Mica Lake, south coastal Alaska at c. 2600 cal. yr BP, interpreted to represent the development of more zonal air flow associated with a weakened AL. A zonal air flow pattern in the mid-late Holocene would have translated cooler and drier maritime air to the SBIC and a more northward positioned NPH would have steered cold northeasterly winds into the study region (Klein, 1949). More zonal air-flow would have also reduced the frequency of North Pacific storms because strong temperature gradients would not have been maintained over short distances, and those that did develop would have been translated to the southern coast of BC, resulting in the period of greater precipitation documented at Effingham Inlet (Klein, 1949; Schiff et al., 2009; Hubeny et al., 2011).

5.2.3. The latest Holocene (c. 2056–1791 cal. yr BP to c. 1540–911 cal. yr BP)

Skeletonema costatum decreases in abundance while *Cyclotella choctawatcheeana* and the frequency of occurrences of benthic brackish diatoms (e.g., *Martyana* spp., *Planothidium delicatulum*) increase in the latest Holocene in VEC02A02. *Skeletonema costatum* is common in spring and summer blooms along the coast of BC. *Skeletonema costatum* is light and temperature sensitive; it typically blooms following the initial *Thalassiosira* spp. stage when water temperatures become warmer as the spring/summer season progresses (Sancetta, 1989; Haigh et al., 1992). Its decline at this time suggests that relatively cool climate conditions prevailed. Nutrients are also important for *S. costatum* production and sufficient nutrients must remain in the water column after spring diatom production or be recharged by upwelling and/or terrigenous runoff (Waite et al., 1992), suggesting that nutrient levels following the initial spring bloom were low and not recharged by rare incursions of upwelled seawater or terrigenous runoff (Smayda, 1973; Hitchcock and Smayda, 1977). Frequent occurrences of massive sedimentary successions after c. 1992–1727 cal. yr BP (FSZ-C) in VEC02A04 are likely to have been the result of increased slope failure and re-deposition of basin sediments associated with enhanced sediment flux into Frederick Sound and/or incursions of intermediate-depth waters; both scenarios are expected during a wetter climate regime (Hay et al., 2009). The relatively high abundance of benthic brackish diatoms (e.g., *Martyana* spp., *P. delicatulum*) in FDZ-C also suggest that runoff due to precipitation was high and frequently initiated transport of these diatoms from their shallower water habitats on sides of the fjord to the basin centre. Reduced light incidence associated with increased turbidity may also have impacted diatom assemblages by limiting production of light sensitive *S. costatum*.

A decrease in grain size in FSZ-C despite indications of a wetter climate from other proxies preserved in VEC02A04 cannot be explained within the present investigation. Grain size is poorly correlated to total diatom abundance ($y = -5E-09X + 91.089$, $R^2 = 0.0009$), so it is unlikely that this trend in grain size reflects changing diatom assemblages in Frederick Sound.

An increase in the relative abundance and accumulation rate of Cupressaceae pollen in the upper c. 300 cm (post c. 2413–2183 cal. yr BP) of VEC02A04 also suggests that climate became more humid in the latest Holocene at Frederick Sound (Galloway et al., 2010). In Alison Sound, a decrease in laminae concentration and increase in sedimentary grain size suggest that a return to wetter conditions occurred in the SBIC at c. 1700 cal. yr BP (Patterson et al., 2007). In south coastal BC, warmer and drier climate conditions prevailed after c. 2000 cal. yr BP in Effingham Inlet (Patterson et al., 2004b) and after c. 1750 cal. yr BP at Saanich Inlet (Nederbragt and Thurow, 2001) (Fig. 10).

We interpret the AL to have been positioned relatively eastward, and to have been more intense after c. 2056–1791 cal. yr BP, a configuration that would have diverted storm-tracks northward and resulted in the generally wetter conditions inferred from sediments, diatoms, and pollen (Galloway et al., 2010) in the SBIC in the latest Holocene. After c. 2000 cal. yr BP, ENSO and PDO-like climate variability in the NE Pacific, and associated shifts in the AL and NPH, was enhanced (Barron and Anderson, 2011). The Jellybean Lake oxygen isotope record documents a rapid and high amplitude intensification and/or easternward movement of the AL at c. 1200 cal. yr BP (Anderson et al., 2005). In northern BC, increases in exotic, west-sourced *Tsuga heterophylla* pollen are documented at c. 1950 cal. yr BP at Susie Lake (Spooner et al., 1997) and at c. 1500 cal. yr BP at Pyramid Lake (Mazzucchi et al., 2003), suggesting an especially intensified and/or eastward positioned AL at these times (Fig. 10). Humidity reached a maximum in the southern Yukon Territory between c. 2250 and 1400 cal. yr BP before declining (Fig. 10; Anderson et al., 2005). In southern Alaska, several glacial advances are documented in the past two millennia, including an advance of the Nabesna Glacier that began near c. 2200 cal. yr BP in the Wrangell Mountains (Fig. 10; Wiles et al., 2004), that also provide evidence for relatively humid conditions in these northern regions. The relatively warmer and drier conditions reconstructed for south coastal BC after c. 2000 cal. yr BP would be expected under the scenario of a relatively eastward positioned and/or intense AL and associated meridional airflow pattern (Barron and Anderson, 2011).

5.3. Cyclic variations in primary productivity and hydrology

Proxy records of primary productivity (total diatom abundance and biogenic silica) and hydrology (grain size) preserved in VEC02A04 reveal significant periodicities of c. 42, 53, 60, 70, 82, 89, 241, 243, and

380 yrs (Fig. 7A). We emphasize periodicities of c. 70 yrs and longer because the Nyquist frequency of our time series approaches the periodicities of the highest frequency signals. Period lengths of c. 42 and 243 yrs detected in grain size are similar to those of c. 53 and 241 yrs revealed in the biotic proxies. The replicability of these signals in grain size, a proxy inferred to represent terrestrial, watershed dynamics, and biotic proxies sampled with a different sampling resolution and inferred to reflect different, albeit related, processes, such as nutrient availability, freshwater input, light incidence, and water temperature, for example, suggests an allogenic driver. The absence of the c. 241 and 380 yr signals present in total diatom abundance data from biogenic silica time series is difficult to explain. The relationship between total diatom abundance and biogenic silica is poor ($y = 9E+07x - 9E+07$, $R^2 = 0.42$), suggesting that remains of biosiliceous organisms, such as radiolarians, sponges, and ebridians, are also represented in the VEC02A04 biogenic silica record.

Cross wavelet analyses of total diatom abundance, biogenic silica, and grain size time series with reconstructed sunspot number time series reveal significant common periodicities within c. 42–60, 70–89, 204–243, and 380 yr bands (Fig. 9). This commonality suggests that solar variability influenced late Holocene primary production and hydrology at Frederick Sound on decadal to centennial time scales. Below we compare these significant common periodicities to previous research (Table 2).

Periodicities within c. 42 to 60 yrs documented in total diatom abundance, biogenic silica, and grain size time series from Frederick Sound and reconstructed sunspot number are correlative with the pentadecadal frequency of the PDO (Minobe, 1999, 2000). Signals of 42–60 yrs are approached by Nyquist frequencies of 26 yrs (grain size), 52 yrs (total diatom abundance and biogenic silica), and c. 20 yrs (reconstructed sunpost number), so our confidence that periodicities of 42–60 yrs detected in times series are real is lower than for the lower frequency signals. Periodicities within 42–60 yrs have been previously reported from a late Holocene record of primary productivity from Effingham Inlet and are coherent with inferred changes in the relative position and intensity of the AL (Anderson et al., 2005; Ivanochko et al., 2008). Frequencies of c. 42–60 yrs are also documented in far distant sites, such as in the Palmer Deep of Antarctica as changes in grain size (Warner and Domack, 2002) and Tasmania as variations in tree-ring thickness (Cook et al., 1996), suggesting a global-teleconnection mechanism for the PDO and/or celestial forcing. A c. 60 yr periodicity is also present in a 68–70 Ma yr old record of tree ring width from Alberta (Raspopov et al., 2011).

Periodicities within 70 to 89 yrs that occur in total diatom abundance, biogenic silica, and reconstructed sunspot number time series are also present as changes in marine sedimentation in nearby Alison Sound and in primary production, fish population dynamics, and sedimentation in Effingham Inlet (Patterson et al., 2004b, 2005, 2007; Ivanochko et al., 2008). Similar frequencies are documented in a wide array of proxy records from far distant sites, including in the spatial pattern of sea surface temperature in the North Atlantic, storminess in the eastern Norwegian Sea, instrumental observations of oceanic upwelling along the Iberian Peninsula coast, sedimentation in the Palmer Deep, Antarctica, and temperature and carbon cycling in the Ionian Sea (Castagnoli et al., 1992; Warner and Domack, 2002; Sarnthein et al., 2003; Lohmann et al., 2004; Asmerom et al., 2007; Berner et al., 2010; Santos et al., 2011). On land, a c. 70–100 yr cycle is observed in tree-ring records from Tasmania and precipitation patterns across the United States (Cook et al., 1996; Ware and Thomson, 2000; Asmerom et al., 2007). In the geologic record, a c. 96 yr periodicity is documented in a 250-million yr old varve thickness record from the Castile Formation of west Texas (Dean, 2000) and c. 80 and 120 yr periodicities are documented in proxy records of Late Miocene climate from Paleo-Lake Pannon, Vienna Basin (Kern et al., 2012). A c. 90 yr signal is also replicated in proxies of solar activity (Suess, 1980; Stuiver and Braziunas, 1993; Beer et al., 2000; Peristykh and Damon, 2003), documented in naked-eye sunspot observations between the yrs 1610 and 1980 AD (Hoyt and Schatten, 1993; Lean et al., 1995), and is correlative to the well documented c. 70–100 yr Gleissberg sunspot cycle (Gleissberg, 1971; Garcia and Mouradian, 1998).

The c. 204–243 yr signal present in total diatom abundance, grain size, and reconstructed sunspot number time series are also documented in regional paleoclimate records. A c. 200–250 yr cycle is evident as changes in marine sedimentation and fish populations in Effingham Inlet (Patterson et al., 2004a, 2004b, 2005). A similar cycle of c. 210 yrs occurs in charcoal accumulation rates from Dog Lake, BC (Hallett et al., 2003). A c. 200 yr cycle affected lacustrine paleoproductivity and summer temperatures in Alaska (Hu et al., 2003; Wiles et al., 2004). In far distant sites, a c. 200–250 yr cycle is present in terrestrial, marine, lacustrine, and ice proxy records of temperature, precipitation, ocean circulation, and atmospheric circulation (Anderson, 1992; Castagnoli et al., 1992; Cook et al., 1996; Yu and Ito, 1999; Ram and Stolz, 1999; Matthews et al., 2000; Cooper et al., 2000; Bond et al., 2001; Haug et al., 2001; Wagner et al., 2001; Poore et al., 2003, 2004; Springer et al., 2008; Raspopov et al., 2008; Swindles et al., 2012). The c. 200 yr periodicity is also present as changes in varve thickness in the Permian Castile Formation (Dean, 2000) and manifested as variations in tree-ring thickness in the 68–70 Ma yr old cypress stump record from Alberta (Raspopov et al., 2011). During both periods of geologic time, the c. 200 yr cycle was strong enough to modulate the amplitudes of other periodicities (Raspopov et al., 2011). A. c. 208 yr signal also occurs in the Late Miocene-aged paleoclimate record of Paleo-Lake Pannon (Kern

Table 1
Conventional and calibrated radiocarbon ages measured by atomic mass spectrometry from the Frederick Sound sediment core VEC02A04.

Laboratory number	Depth (cm)	Sedimentology	Material dated	Conventional age (^{14}C yr BP)[a]	Calibrated age (cal. yr BP)[b,c]	Median calibrated age (cal. yr BP)[d]
TO-10788	97	Laminated	Wood fragment	1510 ± 60	1306–1523	1414.5 ± 108
TO-11082	313	Massive	Wood fragment	3070 ± 70	3076–3412	3244 ± 168
TO-10789	457	Laminated	Wood fragment	2560 ± 80	2362–2784	2573 ± 211
TO-10790	457	Laminated	Wood fragment	3050 ± 60	3076–3383	3229.5 ± 153.5
TO-11084	734	Woody layer	Conifer cone	2540 ± 70	2432–2759	2595.5 ± 163.5
UBA-13359	945	Laminated	Wood fragment	3318 ± 32	3469–3633	3551 ± 82
TO-10791	1051	Laminated	Twig	4350 ± 80	4816–5093	4954.5 ± 138.5
UBA-13360	1060	Laminated	Wood fragment	3710 ± 22	3981–4094	4037.5 ± 56.5
TO-10793	1182	Massive	Wood fragment	3770 ± 60	3973–4300	4136.5 ± 163.5

[a] ±90% confidence interval.
[b] Range represents 95% confidence interval.
[c] Calibrated using Calib6.0 (Stuiver and Reimer, 1993) and the INTCAL09 dataset (Reimer et al., 2009).
[d] ±95% confidence interval.

Table 2
Comparison of periodicities determined in time series of proxies of primary production and hydrology preserved in the VEC02A04 sedimentary record to previous research.

Periodicity (yr)*	VEC02A04 dataset	Periodicity also reported in the following records
42–60	Total diatom abundance	Pacific North American Index[a]
		Primary production, Effingham Inlet[b]
	Biogenic silica	Grain size, Palmer Deep, Antarctica[c]
		Tree-ring thickness, Tasmania[d]
	Grain size	68–70 Ma tree-ring thickness, Alberta[e]
75–89	Total diatom abundance	$\delta^{18}O$ speleothem, SW USA[f]
		Primary production, Effingham Inlet[b]
	Biogenic silica	Tree-ring thickness, western North America[g]
		Grain size, Palmer Deep, Antarctica[c]
		Tree-ring thickness, Tasmania[d]
		Observed Sunspots 1610–1980[h]
		$\Delta^{14}C$ tree-rings[i]
		Upwelling, Iberian Peninsula[j]
		Fish populations, Effingham Inlet[k]
		Total carbonate deposition, Ionian Sea[l]
		Sea ice formation and storminess, Barents Shelf[m]
		Marine sedimentation, Alison Sound[n]
		250 Ma varve thickness, west Texas[o]
		Late Miocene biotic and abiotic paleoclimate proxies, Vienna Basin[p]
204–243	Total diatom abundance	Primary production, Effingham Inlet[b]
		Sr/Ca and $\delta^{13}C$ in stalagmites, West Virginia[q]
	Grain size	Lacustrine biogenic silica, Alaska[r]
		Ostracod-derived Mg/Ca ratios, interior North America[s]
		Ti content planktic foraminifera, Gulf of Mexico and Cariaco Basin[t]
		250 Ma varve thickness, West Texas[o]
		Drift-ice, North Altantic[u]
		Marine sedimentation, Effingham Inlet[v]
		Lacustrine varve thickness, interior North America[w]
		Grain size, Palmer Deep, Antarctica[c]
		Tree-ring thickness, Tasmania[d]
		Summer temperature, Alaska[x]
		^{10}Be Greenland ice core (25–50 kyr BP)[y]
		$\Delta^{14}C$ tree-rings[i,z]
		Charcoal accumulation rates, BC[aa]
		Sea ice formation and storminess, Barents Shelf[m]
		Fish populations, Effingham Inlet[k]
		Peat humification, Sweden[ab]
		Glacio-lacustrine sedimentation, Norway[ac]
		Marine sedimentation, Baltic Sea[ad]
		Total carbonate deposition, Ionian Sea[l]
		Naked-eye sunspot observations[ae]
		Pollen fluctuations, Italy[af]
		^{10}Be Greenland ice core[ag]
		Peat humification and water tables, Ireland[ah]
		Tree-ring width, Central Asian Mountains[al]
380	Total diatom abundance	Primary production, Effingham Inlet[b]
		Grain size, Palmer Deep, Antarctica[f]
		Hydrological change, interior North America[ai]
		Hydrological change, NW China[aj]
		$\Delta^{14}C$ tree-rings[ak]

* Common power in reconstructed sunspot number time series (Solanki et al., 2004); [a]Dean and Kemp (2004); [b]Ivanochko et al. (2008); [c]Warner and Domack (2002); [d]Cook et al. (1996); [e]Raspopov et al. (2011); [f]Asmerom et al. (2007); [g]Ware and Thomson (2000); [h]Lean et al. (1995); Hoyt and Schatten (1993); [i]Suess (1980), Stuiver and Braziunas (1993), Beer et al. (2000), Peristykh and Damon (2003); [j]Santos et al. (2011); [k]Patterson et al. (2004b); [l]Castagnoli et al. (1992); [m]Sarnthein et al. (2003); [n]Patterson et al. (2007), [o]Dean (2000); [p]Kern et al. (2012); [q]Springer et al. (2008); [r]Hu et al. (2003); [s]Yu and Ito (1999); [t]Haug et al. (2001), Poore et al. (2003, 2004); [u]Bond et al. (2001); [v]Patterson et al. (2005); [w]Anderson (1992); [x]Wiles et al. (2004); [y]Wagner et al. (2001); [z]Stuiver et al. (1998), Peristykh and Damon (2003); [aa]Hallett et al. (2003); [ab]Borgmark (2005); [ac]Matthews et al. (2000); [ad]Kunzendorf and Larsen (2002); [ae]Vaquero et al. (1997); [af]Di Rita (2012); [ag]Usoskin et al. (2004); [ah]Swindles et al. (2012); [ai]Laird et al. (1996); Dean (1997); Fritz et al. (2000); Dean and Schwalb (2000); [aj]Wu et al. (2009); [ak]Stuiver and Braziunas (1989); [al]Raspopov et al. (2008).

et al., 2012). A c. 250 yr periodicity is reported in historical naked-eye observations of sunspots between 165 BC and 1918 AD (Vaquero et al., 1997) and a c. 200 yr cycle is documented as changes in cosmogenic nuclide concentrations in Holocene tree-ring and ice core records spanning the last ice age (Wagner et al., 2001; Vasiliev and Dergachev, 2002; Peristykh and Damon, 2003; Usoskin et al., 2004). The c. 204–243 yr periodicity is temporally correlative to the c. 200 yr Suess/de Vries solar cycle.

Significant common power within c. 42–60, 70–89, and 204–243 yr bands occurs between proxy records of primary production and hydrology from Frederick Sound and reconstructed sunspot number. These frequencies are coherent with regional and global records, occur throughout geological time, and in a variety of proxy climate records. Similar to numerous other studies (e.g., Agnihotri et al., 2011; Kern et al., 2012; Breitenmoser et al., 2012), we therefore conclude that solar variability was a control on late Holocene climate of Frederick Sound at these bandwidths. The c. 241–243 yr periodicity present in total diatom abundance and grain size time series demonstrates strongest coherence to reconstructed sunspot number between c. 2900 cal. yr BP and c. 2000 cal. yr BP, suggesting that solar influence on climate at these frequencies was most important in the mid-late Holocene. This time interval is correlative to FSZ-B when laminated sedimentary successions are most frequently preserved, to FDZ-B when diatom assemblage shifts suggest that freshwater input into Frederick Sound was less than during the preceding and succeeding intervals, to a decline in the abundance of Cupressaceae pollen in VEC02AO4 (Fig. 8; Galloway et al., 2010), to local and regional climate change in the NE Pacific (Nederbragt and Thurow, 2001; Patterson et al., 2007), and to a period when the AL was relatively westward positioned and/or weakened between c. 2800 cal. yr BP and c. 1600 cal. yr BP (Anderson et al., 2005) and at c. 2600 cal. yr BP (Schiff et al., 2009; Fig. 10). A period of maximum solar variability is expected to influence the climate of coastal BC through modulation of the relative position and intensity of the AL (Christoforou and Hameed, 1997). The centre of action of the AL is, on average, approximately 700 km westward of its usual position and sea level pressure is increased by about 1.6 mb during periods of solar maximum across the 11-yr Schwabe solar cycle (Christoforou and Hameed, 1997). A relatively westward positioned and weakened AL would result in fewer North Pacific storms being translated to the north coast of BC and result in relatively dry and cool conditions in the study area that would promote primary productivity in the SBIC (Barron and Anderson, 2011). Conversely, during periods when the AL was on average stronger and in a more easterly position, wet and cloudy conditions would have persisted longer into the spring and summer in the SBIC, reducing surface salinities (via direct precipitation, runoff, enhanced freshet) and light incidence; these conditions would have suppressed the spring and summer diatom bloom. A period of high total solar irradiance is also reconstructed between c. 2600 cal. yr BP and c. 1600 cal. yr BP from c. 10,000 yr long reconstructions of solar activity based on ^{10}Be preserved in the GRIP ice core (Vonmoos et al., 2006; Steinhilber et al., 2009). Relatively high amplitude shifts in solar irradiance are a striking feature for the period between c. 3000 cal. yr BP and c. 2250 cal. yr BP in the c. 10,000 yr record of total solar irradiance reconstructed from the INTCAL04 $\Delta^{14}C$ dataset (Vieira et al., 2011).

The c. 380 yr signal present in total diatom abundance time series is non-significant in our analyses of reconstructed sunspot number although cross wavelet transform demonstrates significant common power at this period. A similar c. 320 yr period is also represented as changes in primary production in Effingham Inlet and is coherent with dynamics in the relative position and intensity of the AL inferred from the Jellybean Lake oxygen isotope record (Anderson et al., 2005; Ivanochko et al., 2008). A 360 yr period in tidal mixing may be driven by lunar orbital variability (Keeling and Whorf, 2000). This influence may weakly affect primary production in Effingham Inlet since tidal mixing affects the penetration of oceanic waters into inner basins of BC fjords, but Frederick Sound is expected to be little influenced by tidal mixing due to its inland location and the Jellybean Lake record

should not be affected by tidal phenomena at all (Ivanochko et al., 2008). The c. 380 yr period is also broadly correlative with a c. 400 yr periodicity in hydrology documented in the interior of North America (Laird et al., 1996; Dean, 1997; Yu and Ito, 1999; Dean and Schwalb, 2000) and NW China (Wu et al., 2009) that have been related to solar forcing (Yu and Ito, 1999; Wu et al., 2009) because cosmogenic isotopes also show a periodicity of c. 400 yrs (Stuiver and Braziunas, 1989).

Cross wavelet transform shows periodicities in total diatom abundance and biogenic silica time series to lag common signals in reconstructed sunspot number, whereas grain size leads (Fig. 8). These phase relationships could reflect error in our age-depth model and/or phase shifts in the environmental response to forcing, threshold events, regionality, and non-linearity and non-stationarity of the climate system due to feedback processes and the changing influence of other forcing mechanisms (White et al., 1997; Wiles et al., 2004; White and Liu, 2008; Raspopov et al., 2008; Breitenmoser et al., 2012).

6. Conclusions

A partially-laminated sediment record from Frederick Sound in the Seymour-Belize Inlet Complex of the central coast of BC archives millennial-scale changes in primary productivity and hydrology between c. 4571–4331 cal. yr BP and c. 1540–911 cal. yr BP. Changes in diatom assemblages suggest that a relatively dry climate prevailed between c. 3360–3110 cal. yr BP and c. 2056–1791 cal. yr BP and punctuated otherwise wet late Holocene conditions. This event is broadly correlative with an increase in the preservation of laminated sediments between c. 2948–2708 cal. yr BP and c. 1992–1727 cal. yr BP. We suggest that the relative position and intensity of the AL were on average, more westward and/or weaker than usual during the mid-late Holocene, resulting in the relatively dry conditions inferred for the SBIC. Spectral and wavelet analyses of proxies of productivity (total diatom abundance, biogenic silica) and hydrology (grain size) preserved in the Frederick Sound sediment record are compared to reconstructed sunspot number time series using cross wavelet transformation. Significant common power of c. 42–60, 70–89, 241–243, and 380 yrs occurs, suggesting that solar forcing impacted late Holocene primary production and hydrology at Frederick Sound. The c. 241–243 yr signal is most pronounced during the inferred mid-late Holocene dry climate interval between c. 2900 cal. yr BP and c. 2000 cal. yr BP. A relatively more active sun at this time may have influenced the relative position and intensity of atmospheric circulation features in the NE Pacific.

Acknowledgments

This research was supported by an NSERC Strategic Project Grant, an NSERC Discovery Grant, and a Canadian Foundation for Climate and Atmospheric Sciences Grant to RTP, and Canadian Museum of Nature graduate scholarships to JMG and AW. Thank you to G. Alexander for drafting and to R. Thomson, V. Barrie, and A. Dallimore for core collection, ship-time, and logistic and technical support. We wish to thank the staff and crew of the Canadian Coast Guard Ship *Vector*. Maureen Soon, Department of Earth and Ocean Sciences, University of British Columbia, carried out biogenic silica analysis. Freeze drying of samples for diatom analysis was performed by Malcolm Bilz at the Canadian Conservation Institute in Ottawa. The comments and suggestions of Rod Smith (Geological Survey of Canada, Calgary) and two anonymous reviewers improved this manuscript. This manuscript represents Natural Resources Canada Earth Sciences Sector Contribution Series 20110426.

Appendix A. Diatom taxa occurring ≥1% in at least one sample

Taxon	Authority
Achnanthes cf. *A. grana*	Hohn & Hellerman
Achnanthes sp. 2	
Actinoptychus sp.	
Bacillaria paxillifer	(O.F. Müller) Hendey 1951
Cyclotella caspia	Grunow
Cyclotella choctawatcheeana	Prasad 1990
Cyclotella litoralis	Lange & Syvertsen
Cyclotella stelligera	Cleve and Grunow
Encyonema silesciacum	(Bleisch) D. Mann
Eunotia sp.	
Fragilariopsis cylindriformis	(Hasle in Hasle & Booth) Hasle 1993
Fragilariopsis pseudonana	(Hasle) Hasle 1993
Martyana cf. *M. schulzii*	(Brockmann) Snoeijs
Martyana martyii	(Héribaud) Round
Navicula perminuta	Grunow 1880
Nitzschia frustulum	(Kützing) Grunow in Cleve & Grunow 1880
Nitzschia liebertruthii	Rabenhorst
Nitzschia perminuta	(Grunow) M. Peragallo 1903
Paralia sulcata	(Ehrenberg) Cleve 1873
Planothidium delicatulum	(Kützing) Round & Bukhtiyarova 1996
Skeletonema costatum	(Greville) Cleve 1878
Tabularia tabulata	(C.A. Agardh) Snoeijs 1992
Thalassionema nitzschioides	(Grunow) Mereschkowsky 1902
Thalassiosira decipiens	(Grunow) Jørgensen 1905
Thalassiosira eccentrica	(Ehrenberg) Cleve 1904
Thalassiosira hyalina	(Grunow) Gran 1897
Thalassiosira leptopus	(Grunow) Hasle & Fryxelll 1977
Thalassiosira nordenskioeldii	Cleve 1873
Thalassiosira pacifica	Gran and Angst 1931
Thalassiosira sp. 11	
Thalassiosira sp. 13	
Thalassiosira sp. 17	
Thalassiosira sp. 4	
Thalassiosira sp. 7	
Thalassiosira sp. 8	
Thalassiosira tenera	Proschkina-Lavrenko 1961

References

Agnihotri, R., Dutta, K., Soon, W., 2011. Temporal derivative of Total Solar Irradiance and anomalous Indian summer monsoon: an empirical evidence for a Sun–climate connection. Physics 73, 1980–1987.
Anderson, R.Y., 1992. Possible connection between surface winds, solar activity and the Earth's magnetic field. Nature 358, 51–53.
Anderson, L., Abbott, M.B., Finney, B.P., Burns, S.J., 2005. Regional atmospheric circulation change in the North Pacific during the Holocene inferred from lacustrine carbonate oxygen isotopes, Yukon Territory, Canada. Quaternary Research 64, 21–35.
Asmerom, Y., Polyak, V., Burns, S., Rassmussen, J., 2007. Solar forcing of Holocene climate, new insights from a speleothem record, southwestern United States. Geology 35, 1–4.
Babalola, L.O., 2009. Late Holocene Paleoclimatic and Paleoceanographic Records in Anoxic Basins Along the British Columbia Coast. Carleton University, Ottawa, Canada (Ph.D. Thesis).
Babalola, L.O., Patterson, R.T., Prokoph, A., 2013. Foraminiferal evidence of a late Holocene westward shift of the Aleutian Low pressure system. Journal of Foraminiferal Research 43, 127–142.
Bard, E., Raisbeck, G.M., Yiou, F., Jouzel, J., 1997. Solar modulation of cosmogenic nuclide production over the last millennium: comparison between ^{14}C and ^{10}Be records. Earth and Planetary Science Letters 150, 453–462.
Barron, J.A., Anderson, L., 2011. Enhanced Late Holocene ENSO/PDO expression along the margins of the eastern North Pacific. Quaternary International 235, 3–12.
Batterbee, R.W., Kneen, M.J., 2003. The use of electronically counted microspheres in absolute diatom analysis. Limnology and Oceanography 27, 184–188.
Beer, J., Mende, W., Stellmacher, R., 2000. The role of the sun in climate forcing. Quaternary Science Reviews 19, 403–415.
Berner, K.S., Koç, N., Godtliebsen, F., 2010. High frequency climate variability of the Norwegian Atlantic Current during the early Holocene period and a possible connection to the Gleissberg cycle. The Holocene 20, 245–255.
Blaauw, M., Christen, J.A., 2011. Flexible paleoclimate age-depth models using an autoregressive gamma process. Bayesian Analysis 6, 457–474.
Bond, G., Kromer, B., Beer, J., Muscheler, R., Evans, M.N., Showers, W., Hoffman, B., Lotti-Bond, R., Hajdas, I., Bonani, G., 2001. Persistent solar influence on North Atlantic climate during the Holocene. Science 294, 2130–2136.
Borgmark, A., 2005. Holocene climate variability and periodicities in south-central Sweden, as interpreted from peat humification analysis. The Holocene 15, 387–395.

Breitenmoser, P., Beer, J., Brönnimann, S., Frank, D., Steinhilber, F., Wanner, H., 2012. Solar and volcanic fingerprints in tree-ring chronologies over the past 2000 years. Palaeogeography, Palaeoclimatology, Palaeoecology 313–314, 127–139.
Broecker, W.S., 1994. An unstable superconveyor. Nature 367, 414–415.
Campbell, C., 1998. Late Holocene lake sedimentology and climate change in southern Alberta, Canada. Quaternary Research 49, 96–101.
Campeau, S., Peintiz, R., Hequette, A., 1999. Diatoms from the Beaufort Sea coast, southern Arctic Ocean (Canada). Bibliotheca Diatomologica 42 (J. Cramer, Berlin).
Castagnoli, G.C., Bonino, G., Serio, M., Sonnett, C.P., 1992. Common spectral features in the 5500-year record of total carbonate in sea sediments and radiocarbon in tree rings. Radiocarbon 34, 798–805.
Chang, A.S., 2004. Ultra-high Resolution Sediment Analysis and Diatom Paleoecology from Effingham Inlet, British Columbia, Canada, Implications for Late Holocene Environmental Change. Carleton University, Ottawa, Canada (Ph.D. Thesis).
Chang, A.S., Patterson, R.T., 2005. Climate shift at 4400 years BP, evidence from high-resolution diatom stratigraphy, Effingham Inlet, British Columbia, Canada. Palaeogeography, Palaeoclimatology, Palaeoecology 226, 72–92.
Chang, A.S., Patterson, R.T., McNeely, R., 2003. Seasonal sediment and diatom record from Late Holocene laminated sediments, Effingham Inlet, British Columbia, Canada. Palaios 18, 477–494.
Christen, J.A., Perez, S., 2009. A new robust statistical model for radiocarbon data. Radiocarbon 15, 1047–1059.
Christoforou, P., Hameed, S., 1997. Solar cycle and Pacific 'centers of action'. Geophysical Research Letters 24, 292–296.
Cook, E., Buckley, B.M., D'Arrigo, R.D., 1996. Interdecadal climate oscillations in the Tasmanian sector of the Southern Hemisphere: evidence from tree rings over the past three millennia. In: Jones, J.D., Bradley, R.S., Jouzel, J. (Eds.), Climate Variations and Forcing Mechanisms of the last 2000 years. NATO ASI Ser. Ser. 1, vol. 141. Springer-Verlag, New York, pp. 141–160.
Cooper, M.C., O'Sullivan, P.E., Shine, A.J., 2000. Climate and solar variability recorded in Holocene laminated sediments — a preliminary assessment. Quaternary International 68–71, 363–371.
Cumming, B.F., Wilson, S.E., Hall, R.I., Smol, J.P., 1995. Diatoms from British Columbia (Canada) lakes and their relationship to salinity, nutrients and other limnological variables. Bibliotheca Diatomologica 31 (J. Cramer, Berlin).
Dallimore, A., Thomson, R.E., Bertram, M.A., 2005. Modern to Late Holocene deposition in an anoxic fjord on the west coast of Canada: implications for regional oceanography, climate and paleoseismic history. Marine Geology 219, 47–69.
Davis, J.C., 1986. Statistics and Data Analysis in Geology. John Wiley & Sons, New York.
Dean, W.E., 1997. Rates, timing, and cyclicity of Holocene eolian activity in north-central United States: evidence from varved lake sediments. Geology 25, 331–334.
Dean, W.E., 2000. The sun and climate. USGS Fact Sheet FS-095-00, pp. 1–5.
Dean, J.M., Kemp, A.E.S., 2004. A 2100 year BP record of the Pacific Decadal Oscillation, El Niño Southern Oscillation and Quasi-Biennial Oscillation in marine production and fluvial input from Saanich Inlet, British Columbia. Palaeogeography, Palaeoclimatology, Palaeoecology 213, 207–229.
Dean, W.E., Schwalb, A., 2000. Holocene environmental and climatic change in the Northern Great Plains as recorded in the geochemistry of sediments in Pickerel Lake, South Dakota. Quaternary International 67, 5–20.
Delaygue, G., Stocker, T.F., Joos, F., Plattner, G.-K., 2003. Simulation of atmospheric radiocarbon during abrupt oceanic circulation changes: trying to reconcile models and reconstructions. Quaternary Science Reviews 22, 1647–1658.
Di Rita, F., 2012. A possible solar pacemaker for Holocene fluctuations of a salt-marsh in southern Italy. Quaternary International. http://dx.doi.org/10.1016/j.quatint.2011.11.030.
Favorite, F., Dodimead, A.J., Nasu, K., 1976. Oceanography of the Subarctic Pacific Region, 1960–71. Bulletin, 33. INPFC.
Fisheries and OceansCanada, 2003. Tides, currents and water levels. www.tides.gc.ca.
Fritz, S.C., Ito, E., Yu, Z.C., Laird, K.R., Engstrom, D.R., 2000. Hydrologic variation in the northern Great Plains during the last two millennia. Quaternary Research 53, 175–184.
Galloway, J.M., Babalola, L.O., Patterson, R.T., Roe, H.M., 2010. A high-resolution marine palynological record from the central mainland coast of British Columbia, Canada, evidence for a mid-late Holocene dry climate interval. Marine Micropaleontology 75, 62–78.
Garcia, A., Mouradian, Z., 1998. The Gleissberg cycle of minima. Solar Physics 180, 495–498.
Gleissberg, W., 1971. The probable behaviour of sunspot cycle 21. Solar Physics 21, 240–245.
Green, R.N., Klinka, K., 1994. A field guide to site identification and interpretation for the Vancouver forest region. Land Management Handbook Number 28. BC Min. Forests, Victoria.
Grimm, E.C., 1987. CONISS, a FORTRAN 77 program for stratigraphically constrained cluster analysis by the method of incremental sum of squares. Computers & Geosciences 13, 13–35.
Grimm, E.C., 1993. TILIA v2.0 (Computer Software). Illinois State Museum, Research and Collections Center, Springfield.
Grinsted, A., Moore, J.C., Jevrejeva, S., 2004. Application of the cross wavelet transform and wavelet coherency to geophysical time series. Nonlinear Processes in Geophysics 11, 561–566.
Grossman, A., Morlet, J., 1984. Decomposition of Hardy functions into square integrable wavelets of constant shape. Journal of Society for Industrial and Applied Mathematics Journal of Mathematical Analysis 15, 732–736.
Haigh, R., Taylor, F.J.R., Sutherland, T.F., 1992. Phytoplankton ecology of Sechelt Inlet, a fjord system of the British Columbia coast. I. General features of the nano- and microplankton. Marine Ecology Progress Series 89, 117–134.
Häkansson, H., Hajdu, S., Snoeijs, P., Loginova, L., 1993. *Cyclotella hakanssoniae* Wendker and its relationship to *C. caspia* Grunow and other similar brackish water *Cyclotella* species. Diatomologica Research 8, 333–347.
Hallett, J.G., Matthews, R.W., Walker, R.C., 2003. A 1000-year record of forest fire, drought and lake-level change in southeastern British Columbia, Canada. Holocene 13, 751–761.
Hammer, Ø., Harper, D.A.T., Ryan, P.D., 2001. PAST, paleontological statistics software package for education and data analysis. Palaeontologia Electronica 4, 9 (http://www.palaeo-electronic.org/2001_1/past/issue1_01.htm).
Haug, G.H., Hughen, K.A., Sigman, D.M., Peterson, L.C., Röhl, U., 2001. Southward migration of the Intertropical Convergence zone through the Holocene. Science 293, 1304–1308.
Hay, M.B., Pientiz, R., Thomson, R.E., 2003. Distribution of diatom surface sediment assemblages within Effingham Inlet, a temperate fjord on the west coast of Vancouver Island (Canada). Marine Micropaleontology 48, 291–320.
Hay, M.B., Dallimore, A., Thomson, R.E., Calvert, S.E., Pienitz, R., 2007. Siliceous microfossil record of late Holocene oceanography and climate along the west coast of Vancouver Island, British Columbia (Canada). Quaternary Research 67, 33–49.
Hay, M.B., Calvert, S.E., Pienitz, R., Dallimore, A., Thomson, R.E., Baumgartner, T.R., 2009. Geochemical and diatom signatures of bottom water renewal events in Effingham Inlet, British Columbia (Canada). Marine Geology 262, 50–61.
Hitchcock, G.L., Smayda, T.J., 1977. The importance of light in the initiation of the 1972–1973 winter–spring diatom bloom in Narragansett Bay. Limnology and Oceanography 22, 126–131.
Hoyt, D., Schatten, K., 1993. A discussion of plausible solar irradiance variations, 1700–1992. Journal of Geophysical Research 98, 18895–18906.
Hu, F.S., Kaufman, D., Yoneji, S., Nelson, D., Shemesh, A., Haung, Y.S., Tian, J., Bond, G., Clegg, B., Brown, T., 2003. Cyclic variation and solar forcing of Holocene climate in the Alaskan subarctic. Science 301, 1890–1893.
Hubeny, J.B., King, J.W., Reddin, M., 2011. Northeast US precipitation variability and North American climate teleconnections interpreted from late Holocene varved sediments. Proceedings of the National Academy of Sciences of the United States of America 108, 17895–17900.
Hudgins, L., Friebe, C., Mayer, M., 1993. Wavelet transforms and atmospheric turbulence. Physical Review Letters 71, 3279–3282.
Ivanochko, T.S., Calvert, S.E., Thomson, R.E., Pedersen, T.F., 2008. Geochemical reconstruction of Pacific decadal variability from the eastern North Pacific during the Holocene. Canadian Journal of Earth Sciences 45, 1317–1329.
Keeling, C.D., Whorf, T.P., 2000. The 1,800-year tidal cycle: a possible cause of rapid climate change. Proceedings of the National Academy of Sciences of the United States of America 97, 3814–3819.
Kern, A.K., Harzhauser, M., Piller, W.E., Mandic, O., Soliman, A., 2012. Strong evidence for the influence of solar cycles on a Late Miocene lake system revealed by biotic and abiotic proxies. Palaeogeography, Palaeoclimatology, Palaeoecology 329-220, 124–136.
Klein, W.H., 1949. The unusual weather and circulation of the 1948–1949 winter. Monthly Weather Review 77, 99–113.
Kunzendorf, H., Larsen, B., 2002. A 200–300 year cyclicity in sediment deposition in the Gotland Basin, Baltic Sea, as deduced from geochemical evidence. Geochemistry 17, 29–38.
Laird, K.R., Fritz, S.C., Maasch, K.A., Cumming, B.F., 1996. Greater drought intensity and frequency before AD 1200 in the Northern Great Plains. Nature 384, 552–554.
Latif, M., Barnett, T.P., 1996. Decadal variability over the North Pacific and North America, dynamics and predictability. Journal of Climate 9, 2407–2422.
Lean, J.L., Beer, J., Bradley, R.S., 1995. Reconstruction of solar irradiance since 1610: implications for climate change. Geophysical Research Letters 22, 3195–3198.
Leathers, D.J., Yarnal, B., Palecki, M.A., 1991. The Pacific North-American teleconnection pattern and United States climate. 1. Regional temperature and precipitation associations. Journal of Climate 4, 517–528.
Leinen, M., Cwienk, D., Heath, G.R., Biscaye, P., Kolla, V., Thiede, J., Dauphin, J.P., 1986. Distribution of biogenic silica and quartz in recent deep-sea sediments. Geology 14, 199–203.
Lohmann, G., Rimbu, N., Dima, M., 2004. Climate signature of solar irradiance variations, analysis of long-term instrumental, historical, and proxy data. International Journal of Climatology 24, 1045–1056.
Mann, M.E., Cane, M.A., Zebiak, S.E., Clement, A., 2005. Volcanic and solar forcing of the tropical Pacific over the past 1000 years. Journal of Climate 18, 447–456.
Mantua, N.J., Hare, S.R., 2002. The Pacific decadal oscillation. Journal of Oceanography 58, 35–44.
Maraun, D., Kurths, J., 2004. Cross wavelet analysis: significance testing and pitfalls. Nonlinear Processes in Geophysics 11, 505–514.
Matthews, J.A., Dahl, S.O., Nesje, A., Berrisford, M.S., Andersson, C., 2000. Holocene glacier variation in central Jotunheimen, southern Norway based on distal glaciolacustrine sediment cores. Quaternary Science Reviews 19, 1625–1647.
Mazzucchi, D., Spooner, I.S., Gilbert, R., Osborn, G., 2003. Reconstruction of Holocene climate change using multiproxy analysis of sediments from Pyramid Lake, British Columbia, Canada. Arctic Antarctic and Alpine Research 35, 520–529.
McFadgen, B.G., 1982. Dating New Zealand archaeology by radiocarbon. New Zealand Journal of Science 25, 379–392.
McQuoid, M.R., Hobson, L.A., 2001. A Holocene record of diatom and silicoflagellate microfossils in sediments of Saanich Inlet, ODP Leg 169S. Marine Geology 174, 111–123.
Meidinger, D., Pojar, J., 1991. Ecosystems of British Columbia. Special Report Series No. 6. BC Min. of Forests Research Branch, Victoria.
Miller, A.J., Cayan, D.R., Barnett, T.P., Graham, N.E., Oberhuber, J.M., 1994. The 1976–77 climate shift of the Pacific Ocean. Oceanography 7, 21–26.

Minobe, S., 1997. A 50–70 year climatic oscillation over the North Pacific and North America. Geophysical Research Letters 24, 683–686.
Minobe, S., 1999. Resonance in bidecadal and pentadecadal climate oscillations over the North Pacific, role in climatic regime shifts. Geophysical Research Letters 26, 855–858.
Minobe, S., 2000. Spatio-temporal structure of the pentadecadal variability over the North Pacific. Progress in Oceanography 47, 381–408.
Morlet, J., Arens, G., Fourgeau, E., Giard, D., 1982a. Wave propagation and sampling theory — part 1: complex signal and scattering in multilayered media. Geophysics 47, 203–221.
Morlet, J., Arens, G., Fourgeau, E., Giard, D., 1982b. Wave propagation and sampling theory — part 2: sampling theory and complex waves. Geophysics 47, 222–236.
Mortlock, A., Froelich, P.N., 1989. A simple method for the rapid determination of biogenic opal in pelagic marine sediments. Deep Sea Research Part A: Oceanographic Research Papers 36, 1415–1426.
Murray, M.R., 2002. Is laser particle size determination possible for carbonate-rich lake sediments? Journal of Paleolimnology 27, 173–183.
Nederbragt, A.J., Thurow, J.W., 2001. A 6000 yr varve record of Holocene climate in Saanich Inlet, British Columbia, from digital sediment colour analysis of ODP Leg 169S cores. Marine Geology 174, 95–110.
Oswald, W.W., Anderson, P.M., Brown, T.A., Brubaker, L.B., Hu, F., Lozhkin, A.V., Tinner, W., Kaltenrieder, P., 2005. Effects of sample mass and macrofossil type on radiocarbon dating of arctic and boreal lake sediments. The Holocene 15, 758–767.
Patterson, R.T., Prokoph, A., Chang, A.S., 2004a. Late Holocene sedimentary response to solar and cosmic ray activity influenced by climate variability in the NE Pacific. Sedimentary Geology 172, 67–84.
Patterson, R.T., Prokoph, A., Wright, C., Chang, A.S., Thomson, R.E., Ware, D.M., 2004b. Holocene solar variability and pelagic fish productivity in the NE Pacific. Palaeontologia Electronica 6, 17 (http://palaeo-electronic.org/2004_1/fish2/fish2.pd).
Patterson, R.T., Prokoph, A., Kumar, A., Chang, A.S., Roe, H.M., 2005. Late Holocene variability in pelagic fish scales and dinoflagellate cysts along the west coast of Vancouver Island, NE Pacific Ocean. Marine Micropaleontology 55, 183–204.
Patterson, R.T., Prokoph, A., Reinhardt, E., Roe, H.M., 2007. Climate cyclicity in late Holocene anoxic marine sediments from the Seymour-Belize Inlet complex, British Columbia. Marine Geology 242, 123–140.
Patterson, R.T., Chang, A.S., Prokoph, A., Roe, H.M., Swindles, G.T., 2013. Influence of the Pacific Decadal Oscillation, El Niño-Southern Oscillation and solar forcing on climate and primary productivity changes in the northeast Pacific. Quaternary International (in press).
Pellatt, M.G., Hebda, R.J., Mathewes, R.W., 2001. High resolution Holocene vegetation and climate from Core 1034B, ODP Leg 169S, Saanich Inlet, Canada. Marine Geology 174, 211–222.
Peristykh, A.N., Damon, P.E., 2003. Persistence of the Gleissberg 88-year solar cycle over the last c. 12,000 years, evidence from cosmogenic isotopes. Journal of Geophysical Research 108 (A1), 1003.
Pienitz, R., Fedje, D., Poulin, M., 2003. Marine and non-marine diatoms from the Haida Gwaii Archipelago and surrounding coasts, northeastern Pacific, Canada. In: Lange-Bertalot, H., Kociolek, P. (Eds.), Bibliotheca Diatomologica, Band 48. J. Cramer, Stuttgart (146 pp.).
Poore, R.Z., Dowsett, H.J., Verardo, S., 2003. Millennial-to century-scale variability in Gulf of Mexico Holocene climate records. Paleoceanography 18 (1048), 13. http://dx.doi.org/10.1029/2002/PA000868.
Poore, R.Z., Quinn, T.M., Verardo, S., 2004. Century-scale movement of the Atlantic Intertropical Convergence Zone linked to solar variability. Geophysical Research Letters 31. http://dx.doi.org/10.1029/2004GL019940 L12214.
Ram, M., Stolz, M.R., 1999. Possible solar influences on the dust profile of the GISP2 Ice Core from central Greenland. Geophysical Research Letters 26, 1043–1046.
Raspopov, O.M., Dergachev, V.A., Esper, J., Kozyreva, O.V., Frank, D., Ogurtsov, M., Kolström, T., Shao, X., 2008. The influence of the de Vries (~200-year) solar cycle on climate variations: results from the Central Asian Mountains and their global link. Palaeogeography, Palaeoclimatology, Palaeoecology 259, 6–16.
Raspopov, O.M., Dergachev, V.A., Ogurtsov, M.G., Kolström, T., Junger, H., Dmitriev, P.B., 2011. Variations in climate parameters at time intervals from hundreds to tens of millions of years in the past and its relation to solar activity. Physics 73, 388–399.
Reimer, P.J., Baillie, M.G.L., Bard, E., Bayliss, A., Beck, J.W., Blackwell, P.G., Bronk Ramssey, C., Buck, C.E., Burr, G.S., Edwards, R.L., Friedrich, M., Grootes, P.M., Guilderson, T.P., Hajdas, I., Heaton, T.J., Hogg, A.G., Hughen, K.A., Kaiser, K.F., Kromer, B., McCormac, F.G., Manning, S.W., Reimer, R.W., Richards, D.A., Southon, J.R., Talamo, S., Turney, C.S.M., van der Plicht, J., Weyhenmeyer, C.E., 2009. IntCal09 and Marine09 radiocarbon age calibration curves, 0–50,000 years cal BP. Radiocarbon 51, 1111–1150.
Roe, H.M., Doherty, C.T., Patterson, R.T., Milne, G.A., 2013. Isolation basin records of late Quaternary sea-level change, central mainland British Columbia, Canada. Quaternary International (in press).
Ryves, D.B., Clarke, A.L., Appleby, P.G., Amsinck, S.L., Jeppesen, E., Landkildehus, F., Anderson, N.J., 2004. Reconstructing the salinity and environment of the Limfjord and Vejlerne Nature Reserve, Denmark, using a diatom model for brackish lakes and fjords. Canadian Journal of Fisheries and Aquatic Sciences 61, 1988–2006.
Sancetta, C.A., 1989. Processes controlling the accumulation of diatoms in sediments, a model derived from British Columbian fjords. Palaeogeography 4, 235–251.
Sancetta, C., Calvert, S.E., 1988. The annual cycle of sedimentation in Saanich Inlet, British Columbia, implications for the interpretation of diatom fossil assemblages. Deep-Sea Research 35, 71–90.
Santos, F., Gómez-Gesteira, M., deCastro, M., Álvarez, I., 2011. Upwelling along the western coast of the Iberian Peninsula, dependence of trends on fitting strategy. Climate Research 48, 213–218.
Sarnthein, M., van Kreveld, S., Erlenkeuser, H., Grootes, P.M., Kucera, M., Pflaumann, U., Schulz, M., 2003. Centennial-to-millennial-scale periodicities of Holocene climate and sediment injections off the western Barents shelf, 75°N. Boreas 32, 447–461.
Schiff, C.J., Kaufman, D.S., Wolfe, A.A., Dodd, J., Sharp, Z., 2009. Late Holocene storm-trajectory changes inferred from the oxygen isotope composition of lake diatoms, south Alaska. Journal of Paleolimnology 41, 189–208.
Schulz, M., Mudelsee, M., 2002. REDFIT, estimating red-noise spectra directly from unevenly spaced paleoclimatic time series. Computers & Geosciences 28, 421–426.
Schulz, M., Stattegger, K., 1997. SPECTRUM, spectral analysis of unevenly spaced paleoclimatic time series. Computers & Geosciences 23, 929–945.
Schwarzacher, W., 1993. Cyclostratigraphy and the Milankovitch Theory. Elsevier, Amsterdam, London.
Shen, C., Wang, W.-C., Gong, W., Hao, Z., 2006. A Pacific Decadal Oscillation record since 1470 AD reconstructed from proxy data of summer rainfall over eastern China. Geophysical Research Letters 33, L03702.
Smayda, T.J., 1973. The growth of *Skeletonema costatum* during a winter–spring bloom in Narragansett Bay, Rhode Island. Norwegian Journal of Botany 20, 218–247.
Solanki, S.K., Usoskin, I.G., Kromer, B., Schüssler, M., Beer, J., 2004. Unusual activity of the Sun during recent decades compared to the previous 11,000 years. Nature 431, 1084–1087.
Spooner, I.S., Hills, L.V., Osborn, G.D., 1997. Palynological reconstruction of late Quaternary paleoclimate, Susie Lake, Boundary Ranges, Coast Mountains. Journal of Arctic and Alpine Research 29, 156–163.
Springer, G.S., Rowe, H.D., Hardt, B., Edwards, R.L., Cheng, H., 2008. Solar forcing of Holocene droughts in a stalagmite record from West Virginia in east-central North America. Geophysical Research Letters 35 L177035.
Steinhilber, F., Beer, J., Fröhlich, C., 2009. Total solar irradiance during the Holocene. Geophysical Research Letters 39 L19704.
Stuiver, M., Braziunas, T.F., 1989. Atmospheric ^{14}C and century-scale solar oscillations. Nature 338, 405–408.
Stuiver, M., Braziunas, T.F., 1993. Sun, ocean, climate and atmosphere $^{14}CO_2$: an evaluation of causal and spectral relationships. The Holocene 3, 289–305.
Stuiver, M., Polach, P., 1977. Discussion: reporting of ^{14}C data. Radiocarbon 19, 355–363.
Stuiver, M., Reimer, P.J., 1993. Extended ^{14}C data base and revised CALIB 3.0 ^{14}C age calibration program. Radiocarbon 35, 215–230.
Stuiver, M., Reimer, P.J., Bard, E., Beck, J.W., Burr, G.S., Hughen, K.A., Kromer, B., McCormac, G., van der Plicht, J., Spurk, M., 1998. INTCAL98 radiocarbon age calibration. Radiocarbon 40, 1041–1083.
Suess, H.E., 1980. The radiocarbon record in tree rings of the last 8000 years. Radiocarbon 22, 200–209.
Swindles, G.T., Patterson, R.T., Roe, H.M., Galloway, J.M., 2012. Evaluating periodicities in peat-based climate proxy records. Quaternary Science Reviews 41, 57–66.
Thomson, R.E., 1981. Oceanography of the British Columbia Coast. Can. Special Pub. Fish. Aquat. Sci., 56 (Ottawa).
Torrence, C., Compo, G.P., 1998. A practical guide to wavelet analysis. Bulletin of the American Meteorological Society 79, 61–78.
Trenberth, K.A., Hurrell, J.W., 1994. Decadal atmosphere-ocean variations in the Pacific. Climate Dynamics 9, 303–319.
Usoskin, I.G., Mursula, K., Solanki, S.K., Schüssler, M., Alanko, K., 2004. Reconstruction of solar activity for the last millennium using ^{10}Be data. Astronomy and Astrophysics 413, 745–751.
van Hengstum, P.J., Reinhardt, E.G., Boyce, J.I., Clark, C., 2007. Changing sedimentation patterns due to historical land-use change in Frenchman's Bay, Pickering, Canada: evidence from high-resolution textural analysis. Journal of Paleolimnology 37, 603–618.
Vaquero, J.M., Gallego, M.C., Garcia, J.A., 1997. A 250-year cycle in naked-eye observations of sunspots. Geophysical Research Letters 29. http://dx.doi.org/10.1029/2002GL014782.
Vasiliev, S.A., Dergachev, V.A., 2002. The c. 2400-year cycle in atmospheric radiocarbon concentration, bispectrum of ^{14}C data over the last 8000 years. Annales de Geophysique 20, 115–120.
Vázquez-Riveiros, N., Patterson, R.T., 2009. Late Holocene paleoceanographic evidence of the influence of the AL and NPH on circulation in the Seymour-Belize Inlet Complex, British Columbia, Canada. Quaternary Science Reviews 28, 2833–2850.
Vázquez-Riveiros, N.A., Babalola, A.O., Boudreau, R.E.A., Patterson, R.T., Roe, H.M., Doherty, C., 2007. Modern distribution of saltmarsh foraminifera and thecamoebians in the Seymour-Belize Inlet Complex, British Columbia, Canada. Marine Geology 242, 39–63.
Velasco, V.M., Mendoza, B., 2008. Assessing the relationship between solar activity and some large scale climatic phenomena. Advances in Space Research 42, 866–878.
Vieira, L.E.A., Solanki, S.K., Krivova, N.A., Usoskin, I., 2011. Evolution of solar irradiance during the Holocene. Astronomy and Astrophysics 531 (id.A6).
Vonmoos, M., Beer, J., Muscheler, R., 2006. Large variations in Holocene solar activity: constraints from ^{10}Be in the Greenland Ice Core Project ice core. Geophysical Research Letters 111 A10105.
Wagner, G., Beer, J., Massarik, J., Muscheler, R., Kubik, P.W., Mende, W., Laj, C., Raisbeck, G.M., Yiou, F., 2001. Presence of the solar de Vries cycle (205 years) during the last ice age. Geophysical Research Letters 28, 303–306.
Waite, A.M., Bienfang, P.K., Harrison, P.J., 1992. Spring bloom sedimentation in a subarctic ecosystem. II. Succession and Sedimentation. Marine Biology 114, 131–138.
Ware, D.M., McFarlane, G.A., 1989. Fisheries Production Domains in the Northeast Pacific Ocean. Effects of Ocean Variability on Recruitment and an Evaluation of Parameters Used in Stock Assessment Modes. Can. Special Pub. Fish. Aquat. Sci., 108 359–379 (Ottawa).
Ware, D.M., Thomson, R.E., 2000. Interannual to multidecadal timescale climate variations in the northeast Pacific. Journal of Climate 13, 3209–3220.

Warner, N.R., Domack, E.W., 2002. Millennial- to decadal-scale paleoenvironmental change during the Holocene in the Palmer Deep, Antarctica, as recorded by particle size analysis. Paleoceanography 17. http://dx.doi.org/10.1029/2000PA000602 (PAL5-1-PAL5-14).

White, W.B., Liu, Z., 2008. Resonant excitation of the quasi-decadal oscillation by the 11-year signal in the Sun's irradiance. Journal of Geophysical Research 113. http://dx.doi.org/10.1029/2006JC004057 C01002.

White, W.B., Lean, J., Cayan, D.R., Dettinger, M.D., 1997. Response of global upper ocean temperature to changing solar irradiance. Journal of Geophysical Research 102, 3255–3266.

Wiles, G.C., D'Arrigo, R.D., Villalba, R., Calkin, P.E., Barclay, D.J., 2004. Century-scale solar variability and Alaskan temperature change over the past millennium. Geophysical Research Letters 31 L15203.

Witkowski, A., Lange-Bertalot, H., Metzeltin, D., 2000. Diatom flora of marine coasts I. In: Lange-Bertalot, H. (Ed.), Iconographia Diatomologica. , 7, pp. 1–925.

Wu, J., Yu, Z., Zeng, H'A., Weng, N., 2009. Possible solar forcing of 400-year wet–dry climate cycles in northwestern China. Climatic Change 96, 473–482.

Yu, Z.C., Ito, E., 1999. Possible solar forcing of century-scale drought frequency in the northern Great Plains. Geology 27, 263–266.